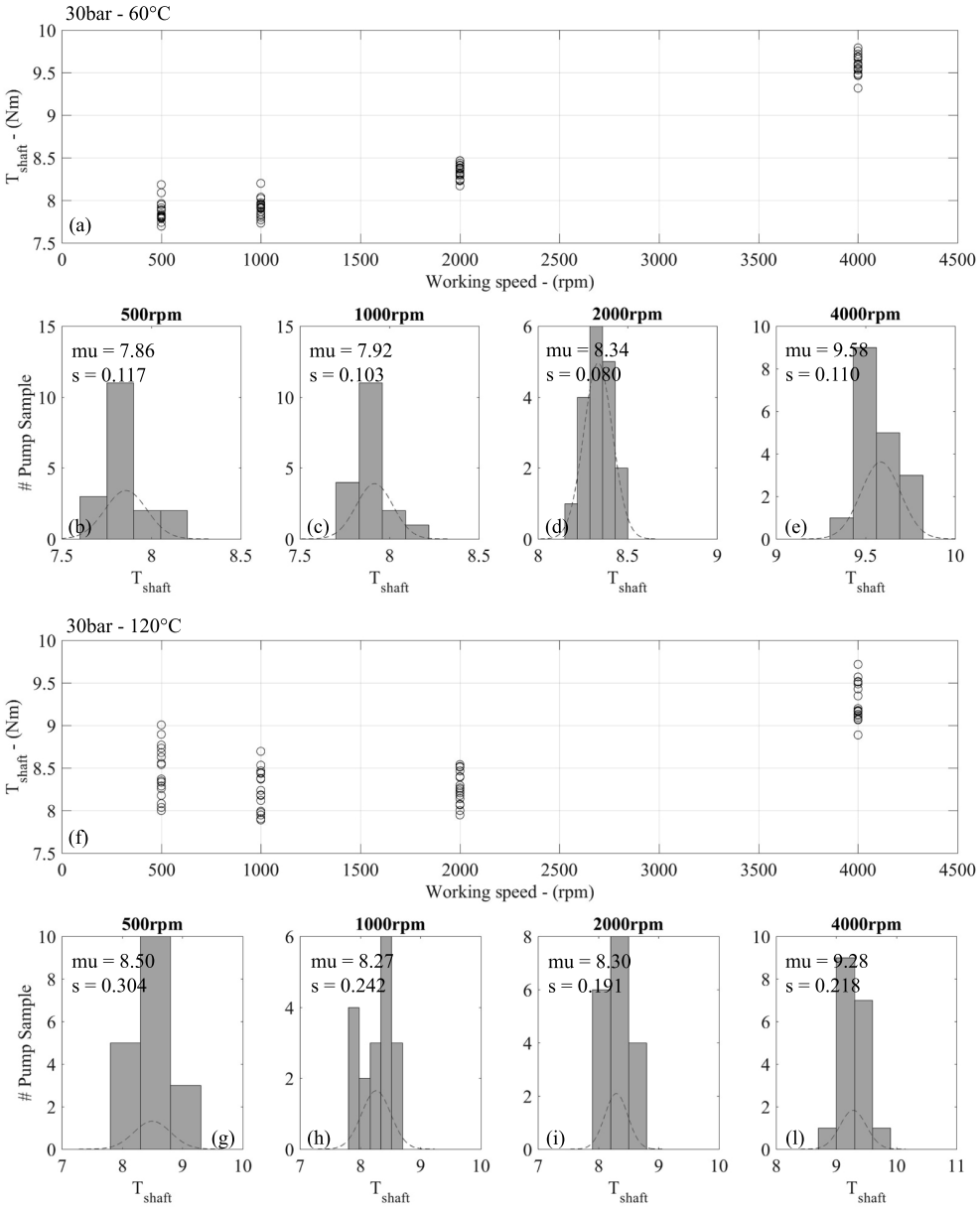

Figure 41: Torque T_{shaft} required to operate the pump with respect to speed variation, for the 20 samples. From (a) to (e), test conditions are: $P_{out} = 30bar$ and $T_{oil} = 60°C$, while from (f) to (l) refer to the same case with $T_{oil} = 120°C$. Data are normally distributed for each analyzed working condition.

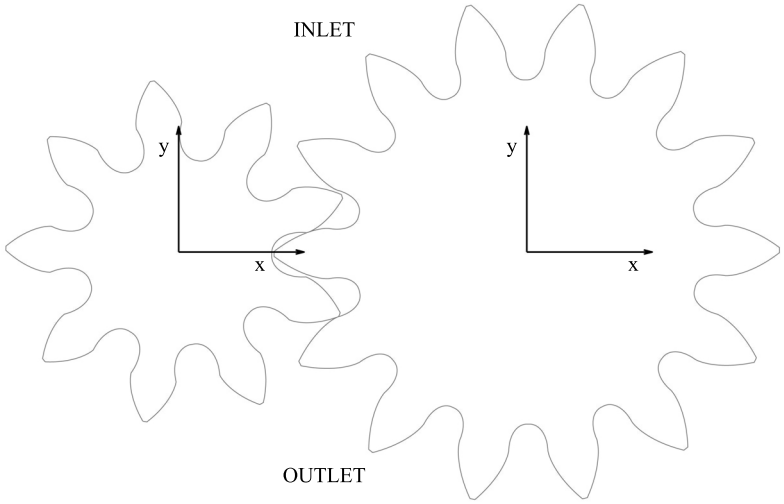

Figure 42: Reference system for the results shown in the present Section.

should be followed if a number of samples is available; in this condition, since Figures 36 and 37 have demonstrated that the mean measured values may deviate considerably from the relative design values, the set up of the model should be based on the mean values of the actual geometrical parameters of the samples. This method would allow to simulate the performance of an average pump (in a statistical sense) and results should be evaluated with respect to the mean experimental data and their relative confidence interval. In presence of a set of samples, validation may also be performed by simulating the entire set of experiments, so that each measured datum can be compared with the relative simulated result. This latter approach appears to be the more complete and rich of information about the effective capabilities of the model; however, the computational effort requested by this validation process tends to overflow as the number of samples increases. Despite these considerations on the effective validation of the model may seem obvious, the three discussed approaches are rarely followed in the literature related to volumetric pumps and model validation is often conducted by direct comparison of the simulated results with measured data taken from a single sample (see for example [45, 9, 35, 81, 82]).

In order to perform an accurate evaluation of the model reliability, the last validation approach described in the previous paragraph has been carried out. Each pump sample has been reproduced and their behavior throughout the

16 different working conditions defined in Table 9 has been numerically simulated. Figures 43 and 44 report the comparison between the simulated and measured characteristic curve of each pump sample, obtained at fixed working speed (1000rpm) and four different delivery pressure values. As it can be appreciated, the model may show a different accuracy depending on the pump sample examined (see for example sample N1 and sample N18). Such a result tends to confirm that reliability and accuracy of this kind of models should be evaluated with respect to a population of pumps, since referring to a single pump sample may easily lead to over/under-estimate the quality of the proposed approach. This aspect is made clear further by considering the data reported in Table 10, which describes the relative deviation $e\%$ (expressed in percentage) between simulated and measured efficiency, calculated as:

$$e\% = 100\frac{\eta_v^s - \eta_v^m}{\eta_v^m} \tag{84}$$

where η_v^s and η_v^m represent simulated and measured volumetric efficiency, respectively. As it can be appreciated, the average relative deviation is kept below the 4% limit for each working condition, while the minimum value is kept even below the 1% limit. Such results confirm the proposed modeling approach is able to correctly simulate the pump behavior, even if some samples occasionally lead to lower accuracy values. Finally, it is worth noting that the mean relative deviation of the estimation tends to worsen as the delivery pressure is increased; however, such a trend may depend also on the experimental results, since their standard deviation is shown to increase together with the delivery pressure.

Similar considerations arise by comparing simulated and measured volumetric efficiency of each pump sample, evaluated at a fixed delivery pressure equal to 30bar and 4 different working speed values (see Figures 45 and 46). As noted in the previous paragraph, the model reaches different levels of accuracy depending on the analyzed sample. However, as shown in Table 11, the average relative deviation is always kept within the 4% limit, except for the 500rpm/30bar condition, in which the mean error reaches almost the 10%. On the other hand, the minimum value is particularly satisfactory, being always less than 0.5%.

By focusing the attention on the whole set of working conditions analyzed, the mean relative deviation estimated with Eqn. 84 is equal to 3.164%, which

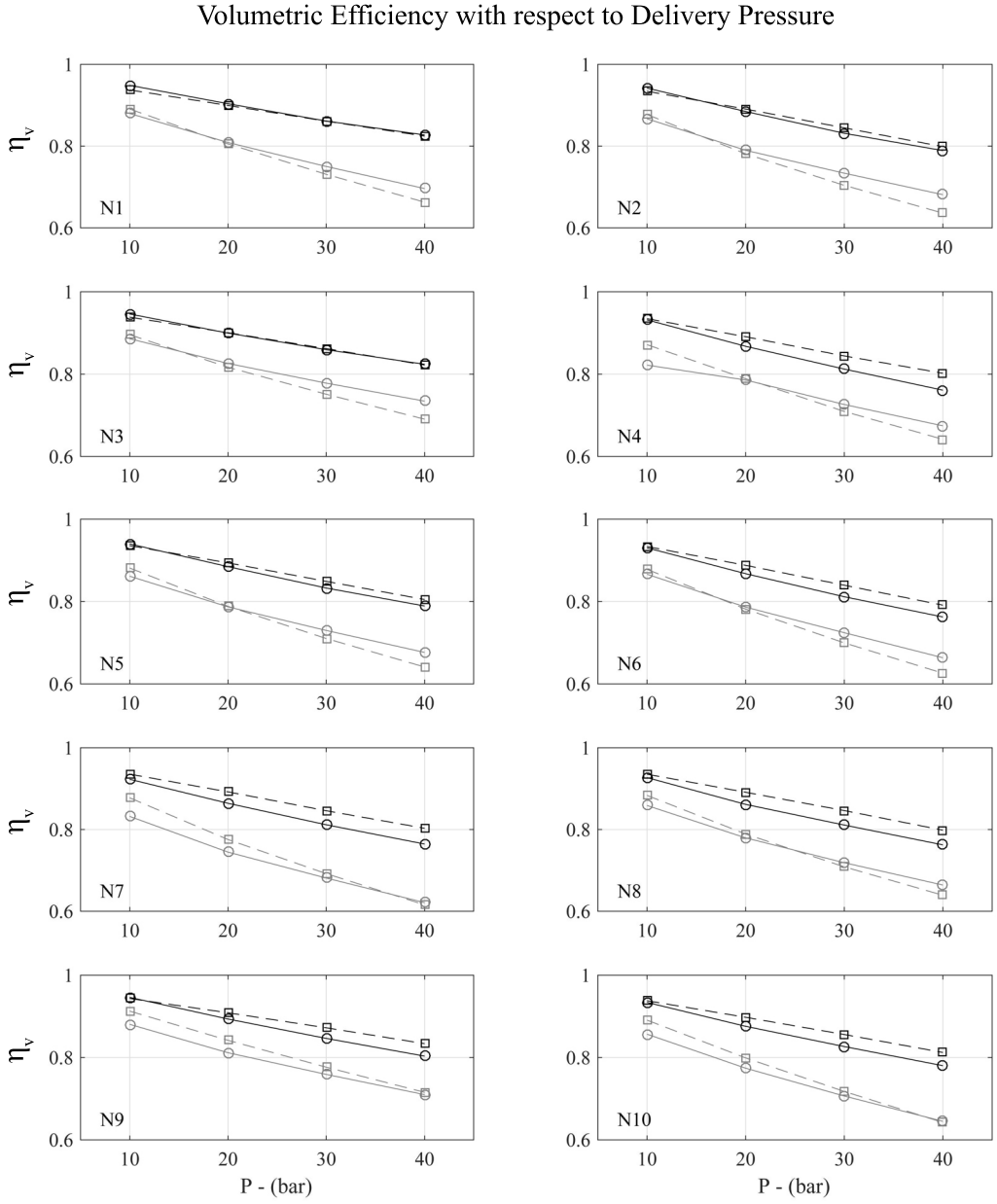

Figure 43: Comparison between simulated (dashed line) and measured (continuous line) volumetric efficiency, with $n = 1000 rpm$ and four different delivery pressure values, for the pump samples from N1 to N10. Black and gray lines refer to oil temperature values equal to $60 degC$ and $120 degC$ respectively.

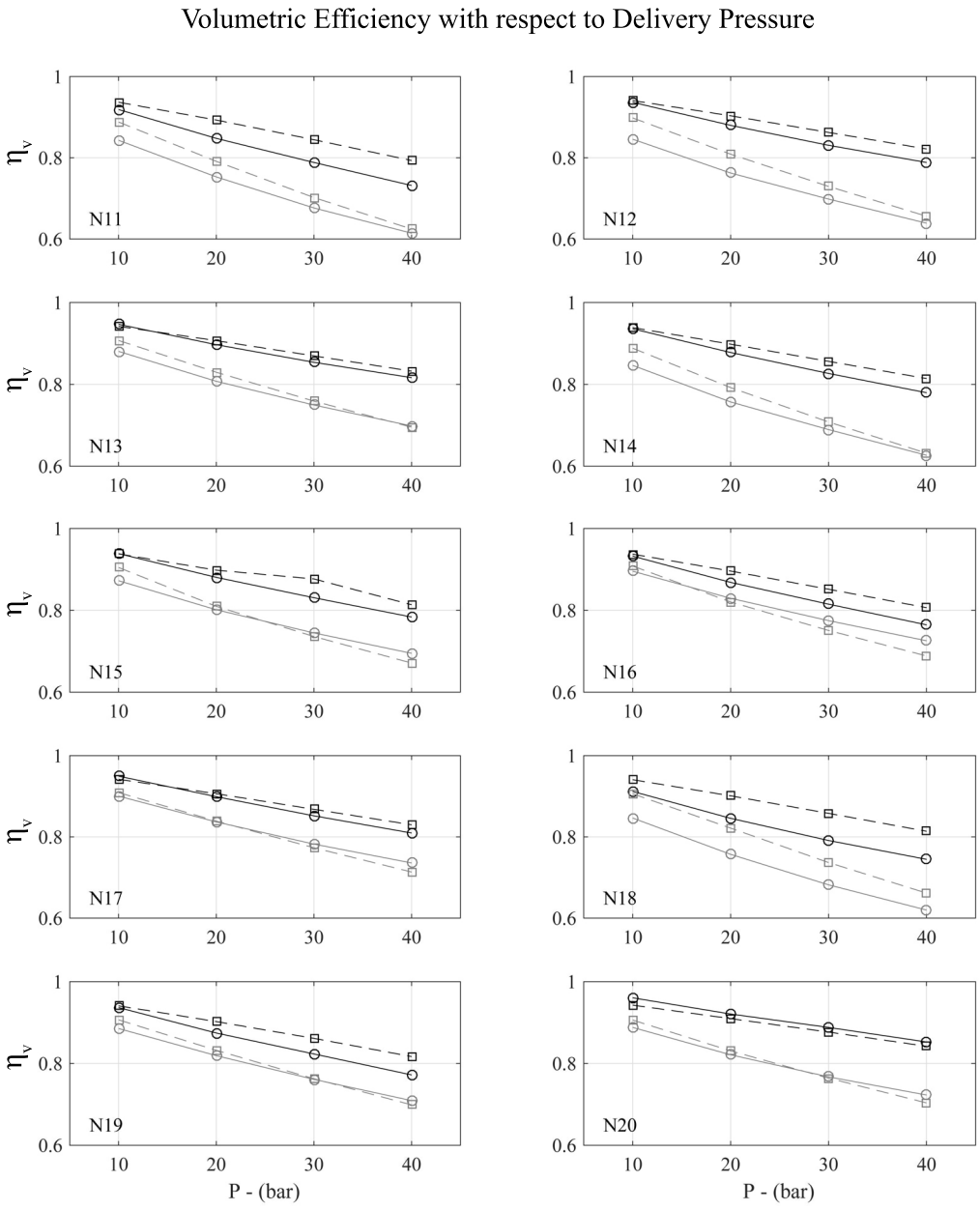

Figure 44: Comparison between simulated (dashed line) and measured (continuous line) volumetric efficiency, with $n = 1000rpm$ and four different delivery pressure values, for the pump samples from N11 to N20. Black and gray lines refer to oil temperature values equal to 60°C and 120°C respectively.

Table 10: Relative deviation between simulated and measured efficiency (in percentage) with respect to delivery pressure variation, calculated on the results shown in Figures 43 and 44.

P_{out}	$e\% - 60°C$			$e\% - 120°C$		
(bar)	**min**	**max**	**mean**	**min**	**max**	**mean**
10	0.07	3.16	0.85	0.97	7.06	3.32
20	0.10	6.55	2.33	0.16	8.53	2.41
30	0.05	8.45	3.45	0.21	8.05	2.58
40	0.21	9.28	3.89	0.41	6.74	3.35

Table 11: Relative deviation between simulated and measured efficiency (in percentage) with respect to working speed variation, calculated on the results shown in Figures 45 and 46.

working speed	$e\% - 60°C$			$e\% - 120°C$		
(rpm)	**min**	**max**	**mean**	**min**	**max**	**mean**
500	0.47	19.00	9.37	0.16	11.95	3.77
1000	0.05	8.45	3.45	0.21	8.05	2.58
2000	0.03	3.12	0.95	0.31	4.13	1.68
4000	0.10	4.54	1.21	0.04	2.08	0.99

is considered to be absolutely satisfying with respect to the rather large set of working conditions analyzed. Finally, it should also be noted that the oil temperature does not seem to influence the model accuracy consistently.

In order to achieve a complete overview of the model reliability, comparison has been also carried out with respect to the average pump, i.e. the pump in which each geometrical parameter is the mean value of the measurements performed on the 20 samples. By following this idea, the average pump geometry results to be defined by the design values, except for tooth-tip/casing clearances and bearing radial clearances, that are defined by the mean values of the measurements reported in Figures 36 and 37. Such a pump has been reproduced inside the numerical model and its behavior has been simulated throughout the whole set of 16 working conditions. Results have been then

compared with the mean value of the measured data at each working condition, together with their 98% confidence interval calculated as:

$$P\left(\bar{x} - t_{\alpha/2,n-1}/\sqrt{n} \leqslant \mu \leqslant \bar{x} + t_{\alpha/2,n-1}/\sqrt{n}\right) = 1 - \alpha \tag{85}$$

where α is the confidence level, i.e. 0.98, n is the number of observations, μ is the mean value of the measured volumetric efficiency for each working condition and $t_{\alpha/2,n-1}$ is the Student's t-distribution value for the given parameters. Figure 47 reports the resulting comparison at different delivery pressure values, while Figure 48 refers to the resulting comparison in terms of different working speed values. As it can be appreciated from both charts, the simulated efficiency falls within the confidence interval for all the 16 analyzed cases. Moreover, as previously noted, influence of the oil temperature on the model accuracy is not detected. The comparison between measured and simulated results presented from Figure 43 to Figure 48 demonstrates that the proposed model is capable to provide a high accuracy estimation of the pump volumetric efficiency, even if it is based on a lumped parameter approach. Such a quality is given by the model capability to couple the pump fluid dynamics with the gearpair micromotions, which take into account not only the variable pressure loads, but also the journal bearing reaction, as well as the mesh force and the speed dependent friction torque.

Despite volumetric efficiency is a fundamental parameter in evaluating gear pump performance, designer are usually interested in having a wider and more detailed overview of the machine behavior. In this context, the present model is able to provide a wide range of data that can help to rate the pump design under study. One of the typical results that can be obtained from this kind of models is given by the oil pressure evolution around gears along a complete revolution. In order to evaluate the output produced by the model, it is possible to refer to Figure 49, depicting the oil pressure course around gears along a complete revolution of the driving gear, for pump sample N1 working at $n = 1000\mathrm{rpm}$ and $T_{oil} = 60°\mathrm{C}$ and different delivery pressure values. As it can be appreciated, the model follows the oil pressure variation inside a single pocket moving towards all the pump regions: starting from the meshing zone, the pressure rises due to the trapping phenomenon, drops to the inlet pressure value when the trapped volume opens to the inlet chamber and then start rising again when the pocket enters into the pressurizing zone. It is worth noting that the pressure evolution on the driven gear has been

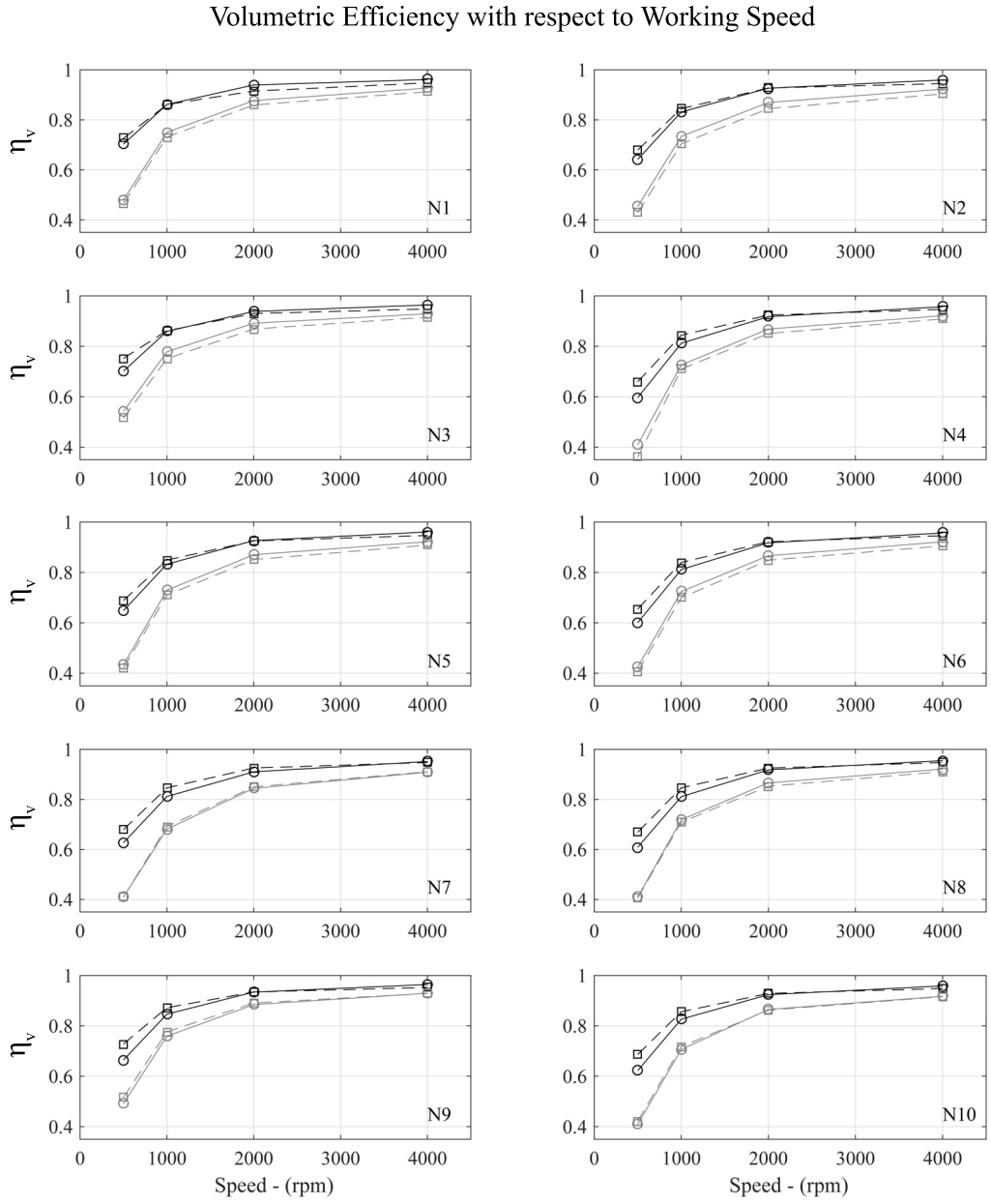

Figure 45: Comparison between simulated (dashed line) and measured (continuous line) volumetric efficiency, with $P_{out} = 30bar$ and four different working speed values, for the pump samples from N1 to N10. Black and gray lines refer to oil temperature values equal to 60°C and 120°C respectively.

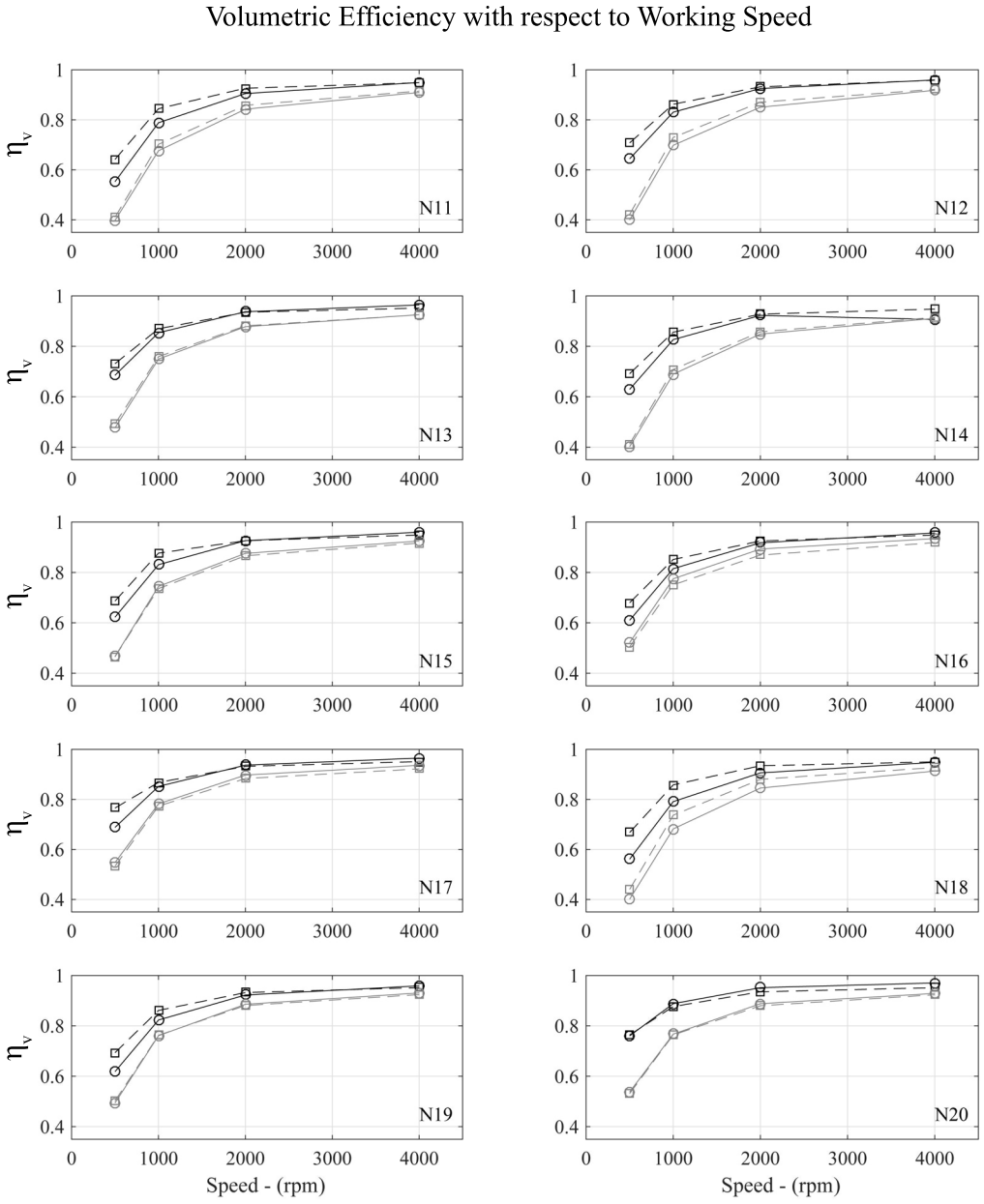

Figure 46: Comparison between simulated (dashed line) and measured (continuous line) volumetric efficiency, with $P_{out} = 30bar$ and four different working speed values, for the pump samples from N11 to N20. Black and gray lines refer to oil temperature values equal to 60°C and 120°C respectively.

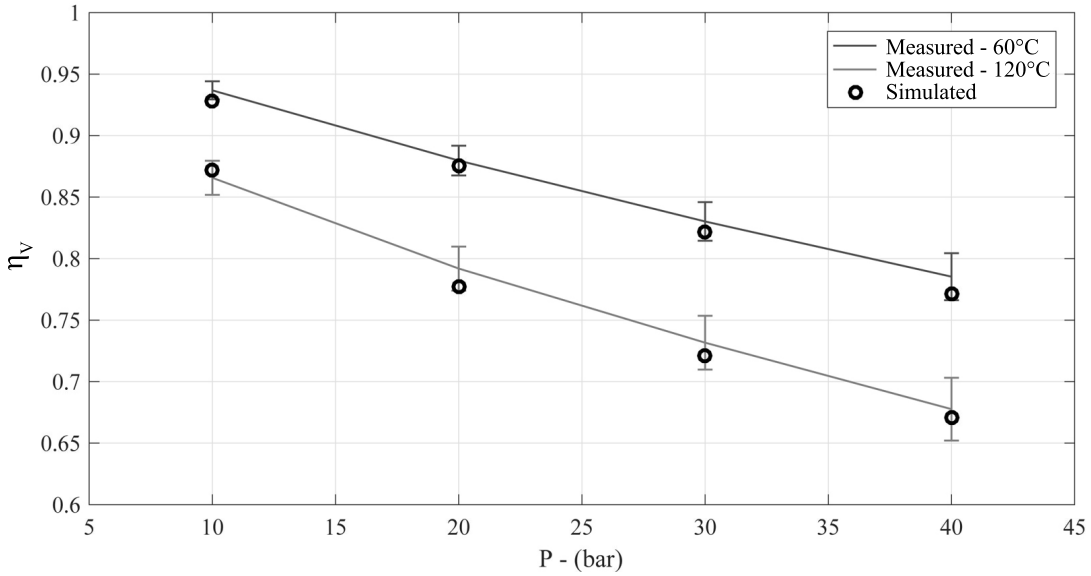

Figure 47: Comparison between average pump simulated efficiency and measured one, with respect to delivery pressure variation. Experimental data are shown as mean value calculated at each working condition, together with their 98% confidence interval calculated with the Student's t-distribution.

plotted with respect to a complete revolution of the driving gear as well, even if it reaches a complete revolution after 9 angular pitches. The data reported in Figure 49, which would require an *ad hoc* test rig to be achieved experimentally [83, 84], may represent a valuable resource to study the effects produced by some design modifications that do not have a clear influence on the outlet pressure ripple or the volumetric efficiency. Concurrently, the analysis of the oil pressure course allows to achieve a deeper understanding of the effects produced by varying the working conditions; a clear example is reported in Figure 50 where the pressure distribution of pump sample N1, working at $P_{out} = 30bar$ and $T_{oil} = 60°C$, is shown at 4 angular speed values. In this case, effects produced by the speed increase is evident both in the meshing zone and the pressurizing zone. In the former, in particular, the speed increment affects the trapping phenomenon by producing a considerable upsurge of the pressure peak, in agreement with the experimental evidence reported in Ref. [8].

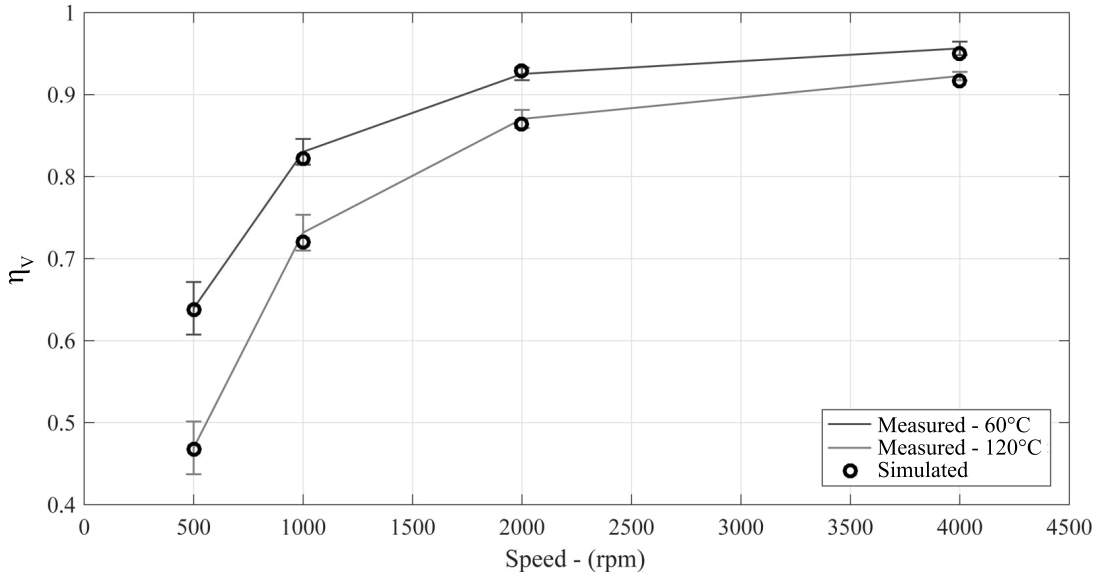

Figure 48: Comparison between average pump simulated efficiency and measured one, with respect to working speed variation. Experimental data are shown as mean value calculated at each working condition, together with their 98% confidence interval calculated with the Student's t-distribution.

The described behavior has important consequences on the variable pressure loads applied to the gears. In Figure 51 it is possible to notice that the presence of high pressure peaks affects both pressure force and torque (data refer to the reference system defined in Figure 42). As a matter of fact, pressure course and loads may be considered as two different ways (or parameters) to analyze the same phenomenon, since pressure loads directly come from the integration of the pressure course around the gearpair surface. However, pressure course is typically more related to a fluid-dynamic point of view; it guarantees an unequivocal correlation between the oil pressure and the gearpair angular position, which allows to detect the potential presence of localized phenomena. On the contrary, pressure loads are generally referred to the dynamics of the machine; they are correlated to the angular pitch and tends to enlighten exclusively the pressure phenomena that may influence the pump balancing or its dynamics. For these reasons, both parameters represent important outcomes available from the model.

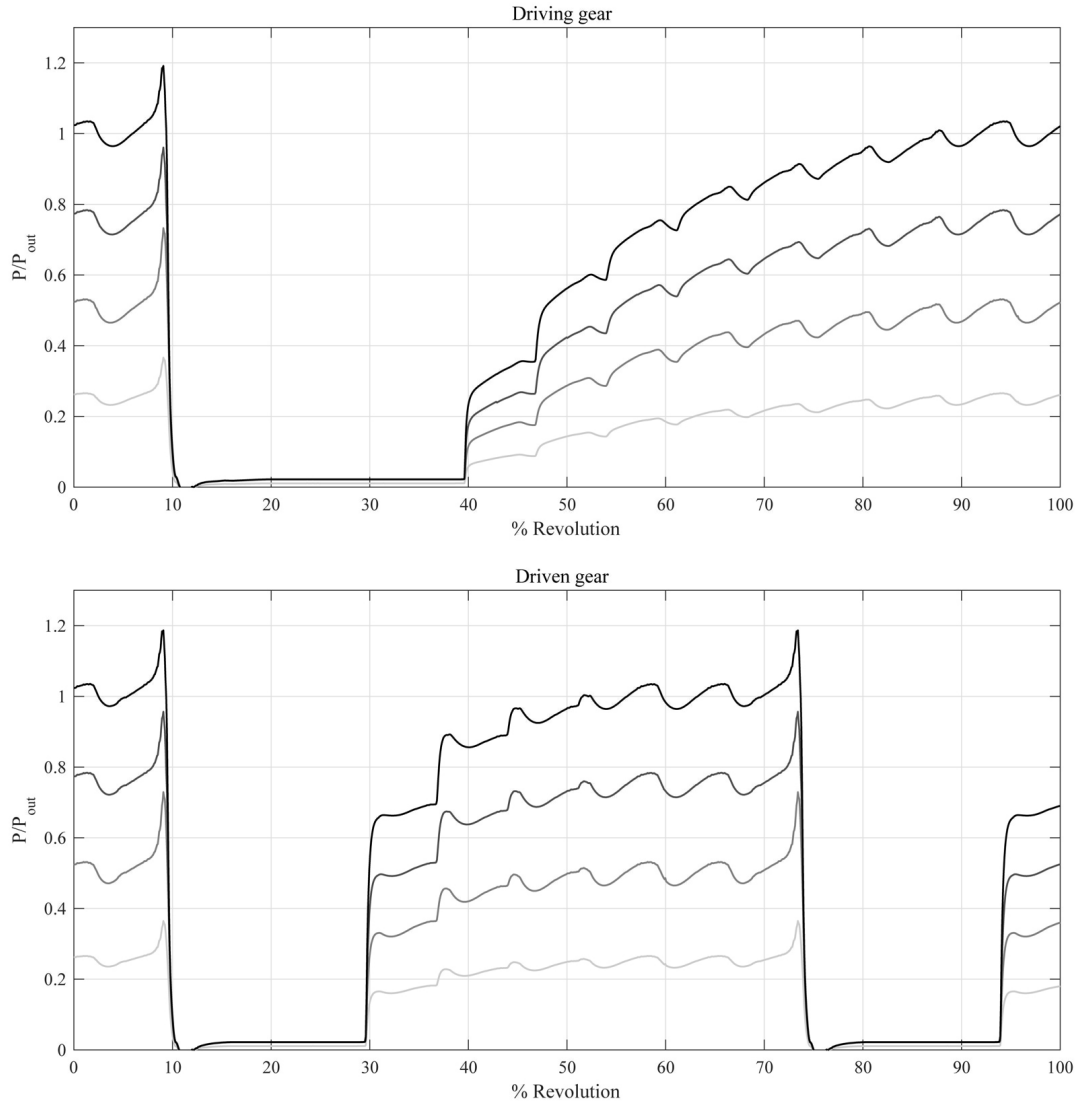

Figure 49: Simulated oil pressure course around gears, referring to pump sample N1, working at $n = 1000rpm$ and $T_{oil} = 60°C$. Data are referred to 4 different delivery pressure values and normalized with respect to $P_{out} = 40bar$.

The analyzed results are classical products obtained from lumped parameter models for simulating gear pump behavior, see for example Refs. [3, 45, 68]. One of the more effective advantages of the present model is actually given by the possibility to produce a number of results to be considered much less

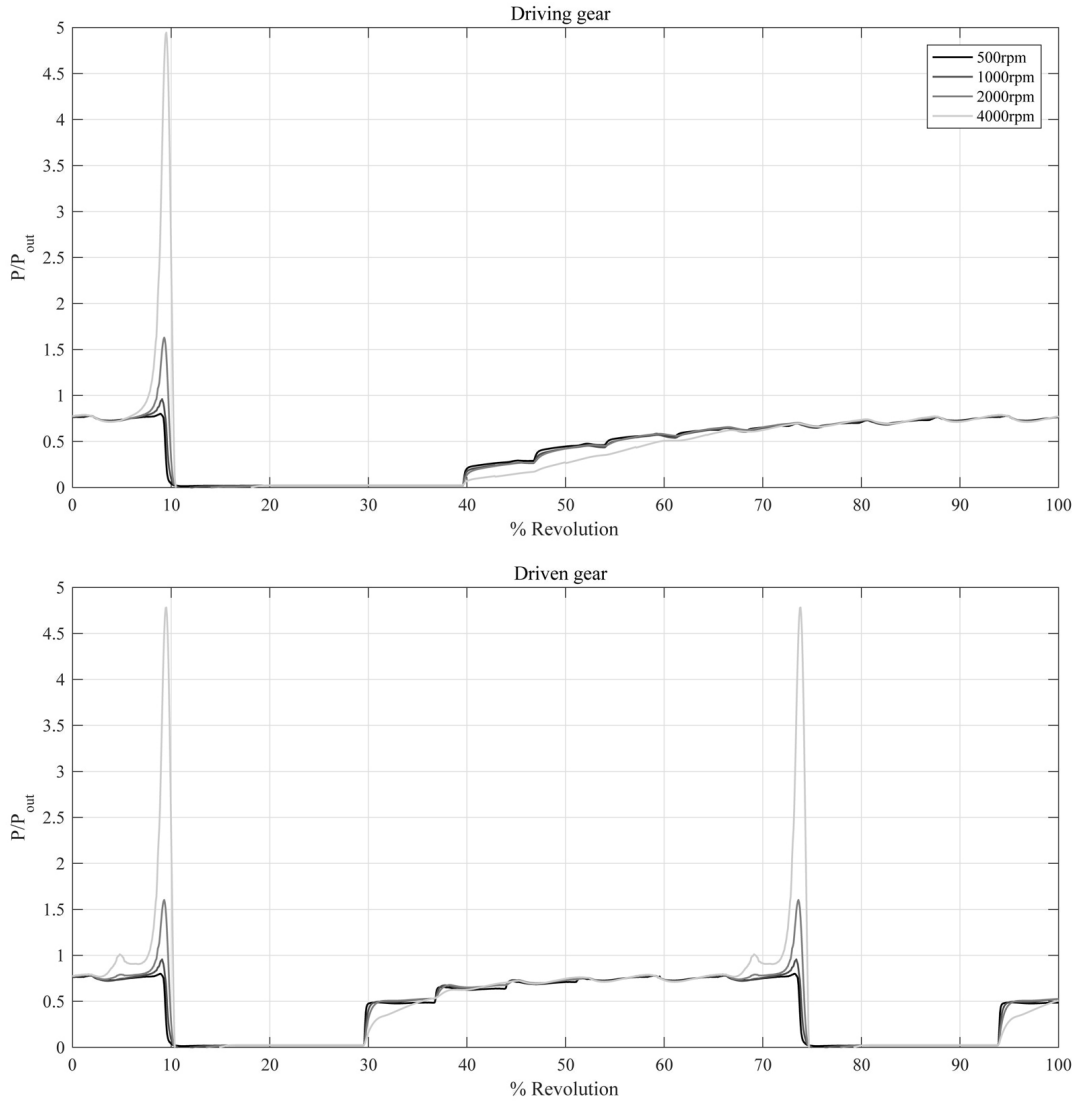

Figure 50: Simulated oil pressure course around gears, referring to pump sample N1, working at $P_{out} = 30bar$ and $T_{oil} = 60°C$. Data are normalized with respect to $P_{out} = 40bar$.

common with respect to the modeling approach adopted, such as time dependent bearing reaction, gear orbits and time/working condition dependent tip clearances. In order to enlighten the model capabilities, bearing reaction for both driving and driven gears is depicted in Figure 52; simulated data refer

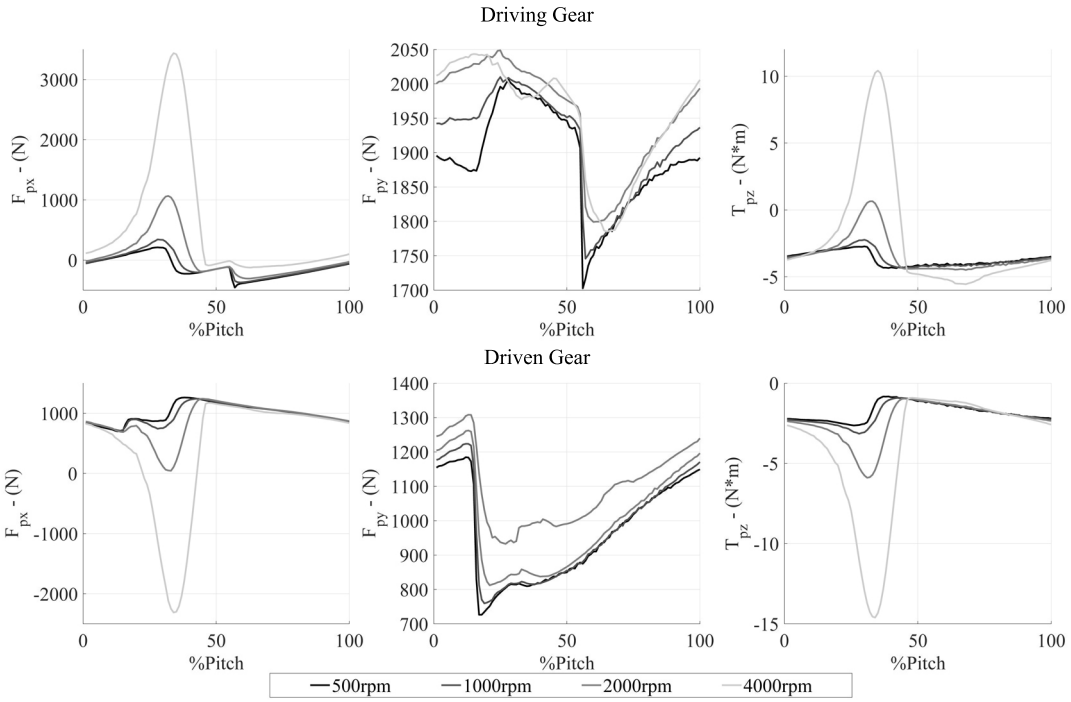

Figure 51: Simulated pressure loads along a complete angular pitch. Data refer to pump sample N1, working at $P_{out} = 30bar$ and $T_{oil} = 60°C$.

to pump sample N1, working at $P_{out} = 30bar$ and $T_{oil} = 60°C$, analyzed at 4 angular speed values. As it can be appreciated, bearing reaction is provided by the model as vector, hence both magnitude and phase can be analyzed. Again, it is worth noting that the high pressure peak due to the trapping phenomenon has consequences also on this parameter. By increasing the working speed, although the mean value of the bearing force magnitude is almost unchanged, a peak starts appearing between the 20% and the 40% of the angular pitch. Moreover, such a phenomenon produces non-negligible effects also on the bearing force phase, demonstrating a change in the direction of application with almost 90° of variation at 4000rpm.

Pressure loads and bearing reaction both contribute in defining the gearpair micromotions, which actually constitute another relevant output provided by the model. In particular, force and torque shown in Figure 51, together with bearing reactions shown in Figure 52, lead to gear center orbits reported in Figure 53. In agreement with the results presented in [20], as the speed is

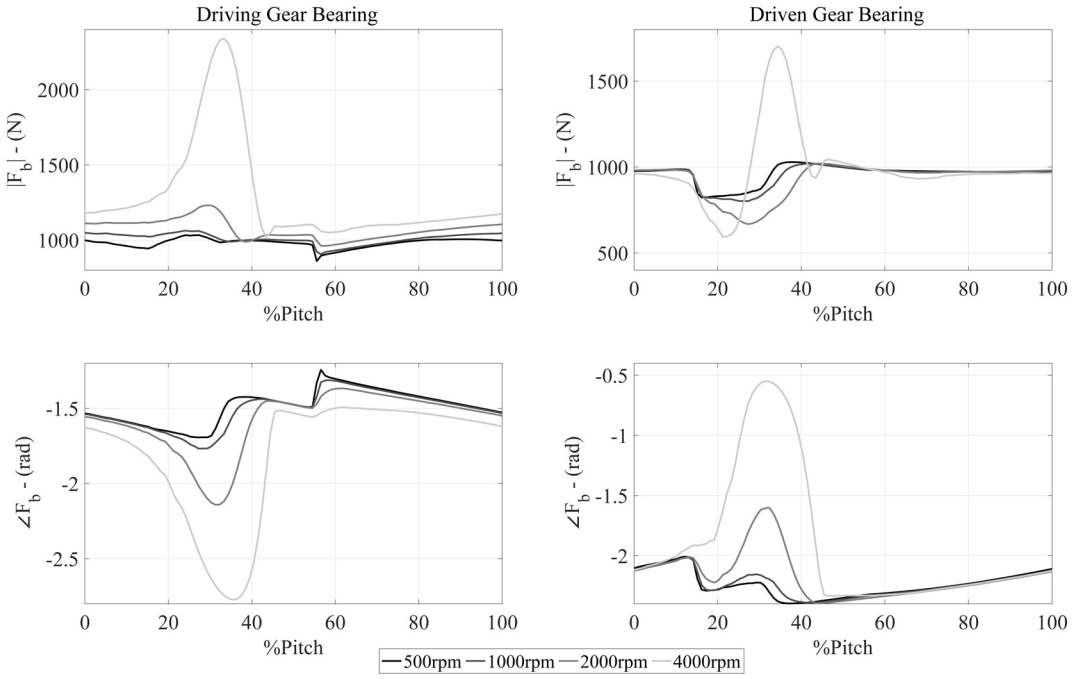

Figure 52: Simulated bearings reactions along a complete angular pitch. Data refer to pump sample N1, working at $P_{out} = 30bar$ and $T_{oil} = 60°C$.

increased, the bearing capability to support the load increases as well, causing each orbit to move faraway from the boundary circle. Such a progressive movement makes the actual tooth tip/casing clearances increase and therefore reduces the sealing capability of the pressurizing zone. This phenomenon well explain the progressive reduction of the oil pressure inside the pressurizing zone due to the speed increase, as shown in Figure 50. Taking as reference the $n = 4000rpm$ case, it is also possible to notice that the high pressure peak inside the pressurizing zone actively concurs in the development of this behavior. Within this working condition, the gearpair is forced to over-enlarge its obits with a further deterioration of its sealing capability. The process is well addressed in Figure 54, which describes the predicted driving gear tooth tip/case clearances along a complete revolution. In particular, such a clearance is shown to assume higher values in the $n = 4000rpm$ case between the 4^{th} and the 6^{th} angular pitch, i.e. at the beginning of the pressurizing zone.

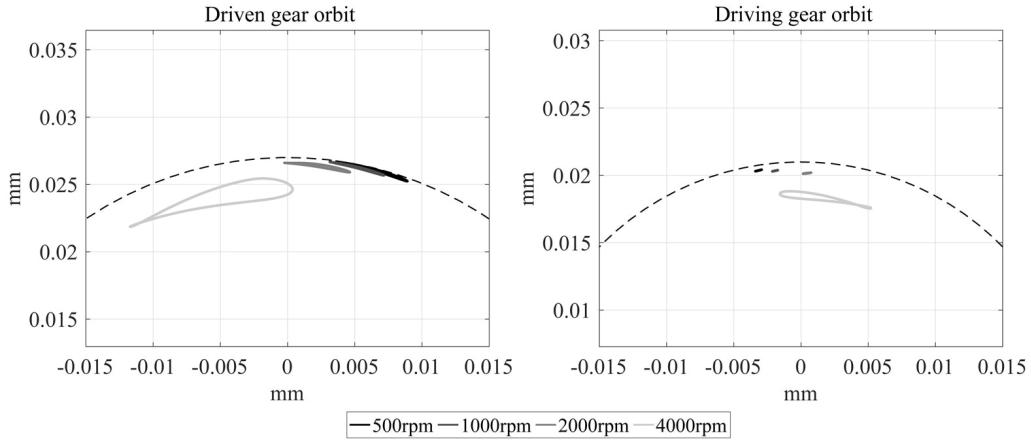

Figure 53: Simulated gear center orbits along a complete angular pitch. Data refer to pump sample N1, working at $P_{out} = 30bar$ and $T_{oil} = 60°C$.

The proposed analysis demonstrates that despite the high pressure peak in the trapping zone and the sealing capability reduction in the pressurizing zone may appear as two distinct phenomena, they are actually correlated. The possibility to explain such a correlation underlines the potentiality of the proposed modeling approach, which allows to analyze the machine behavior from multiple points of view. This characteristic assumes a particular value in the field of gear pumps, where the overall machine behavior is the result of the mutual interaction between different phenomena arising from design aspects that may appear uncorrelated at first.

3.9 CONCLUDING REMARKS

The present Chapter describes a numerical model for the high accuracy prediction of gear pump performance based on a lumped parameter approach, together with its practical application. The novelty of the model resides in the coupling between the effects produced by the fluid-dynamic field and the gearpair micromotions, which are reciprocally solved, at each time-step, to obtain a precise estimation of the machine behavior. The setup of the model takes advantage of the results provided by a 2D CFD model and two 3D CFD models specifically built up to execute the tuning of some parameters as the flow discharge coefficients. The 2D CFD model has permitted to study the

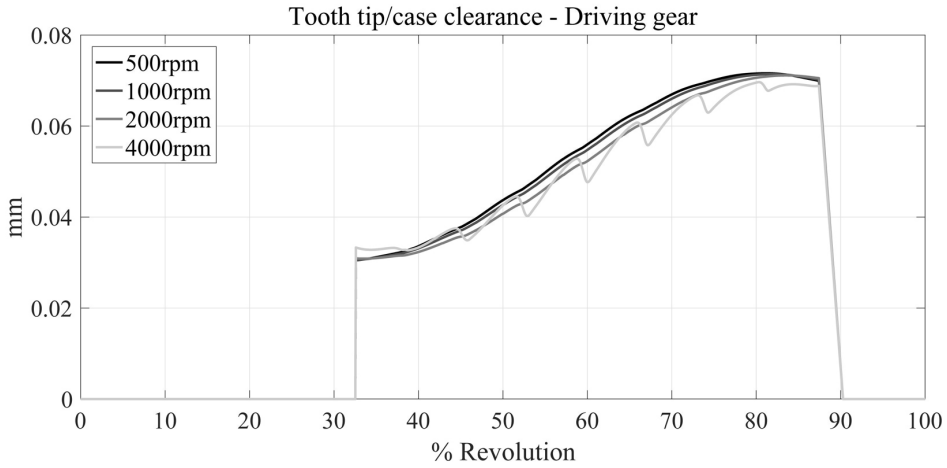

Figure 54: Simulated driving gear tooth-tip/case clearances along a complete revolution. Data refer to pump sample N1, working at $P_{out} = 30bar$ and $T_{oil} = 60°C$.

flow rates exchanged above the tooth tip, while a first 3D CFD model has been used to analyze the flow rate exchanged in the lateral tooth flanks clearance. The second 3D CFD model has been adopted to deeply analyze the meshing region in different instants of meshing and to identify the suitable values of the discharge coefficients to be used in the LP model. Moreover, the mathematical model adopted to solve the gearpair radial movements is based on a detailed set of equations of motion, which is shown to give a more accurate definition of the different loads applied to the gears in comparison to the two approaches already proposed in the literature (see Refs. [17, 35]), by taking into account multiple load sources such as the presence of speed dependent friction torque.

The quality of the estimation is also due to the adoption of a dedicated analytical methodology for the calculation of pressure forces and torques in both spur and helical gear pumps. The methodology consists in a systematic and general procedure to consider the major number of phenomena that characterize the meshing evolution. In order to assess its effectiveness, the method has been applied to both a spur and a helical gear pump and compared with other methodologies available in the literature. The comparison has shown that the determination of pressure force and torque transmitted to the gears is strongly influenced by a number of phenomena occurring inside

the meshing zone, which are taken into consideration by the proposed model. The methodology applied to the helical gears stage enables to estimate all the force and torque components. The obtained results have shown that the pressure force along the axial direction, depending on the helix angle which is usually around 10° in gear pumps, is characterized by a magnitude 10 times lower than the magnitude of the pressure force along the other two directions. Moreover, the shape of helical gears leads to the presence of non-zero components of the pressure torque along axes x and y, even if the magnitude of these components is considerably lower than the pressure torque applied in axial direction. The proposed methodology itself can represent a useful stand-alone tool to precisely estimate one of the main excitation sources that contribute to define the dynamic behavior of these machines.

In order to assess the proposed model, an extended experimental campaign has been carried out on a gear pump designed for automotive applications. The pump design has been reproduced in 20 nominally identical samples, in order to have a statistical characterization of the pump behavior. In addition, tooth tip/case clearances and journal bearing radial clearances have been measured on each sample, with the aim to obtain a more clear definition of their actual geometry. Each sample has been tested on a dedicated test rig, collecting both mean delivery flow rate and driving torque at 16 different working conditions resulted from the combination of 4 delivery pressure values, 4 working speed values and 2 oil temperatures. The complete experimental campaign is therefore constituted by 280 tests. Results obtained from the experimental campaign demonstrate that radial clearances measured at the end of the production process may show high value of the estimated standard deviation, even if such values stand within the design tolerance interval. Moreover, although design limitations are satisfied, slight modifications of the radial clearances may consistently affect the pump performances. Such a phenomenon is amplified as the temperature increases.

Experimental data have been finally adopted to set up the LP model and perform its validation. Each test condition has been simulated for each pump sample, obtaining so 280 different points of comparison, which are not simply based on the working condition, but also on the actual pump geometry. The comparison based on the volumetric efficiency has shown that the model reaches different levels of accuracy depending on the analyzed working condition. However, in terms of delivery pressure dependence, relative

deviation between simulated and measured efficiency is always kept below the 4% limit, while the minimum value is well below the 1% limit. Concurrently, in terms of angular speed dependence, relative deviation is always kept below the 4% limit, except for the 500rpm/30bar condition, in which the mean error reaches almost the 10%. On the other hand, the minimum value is particularly satisfactory, being always less than 0.5%. The comparison enlightens that the model may show different relative error values depending on the pump sample examined; such a result tends to confirm that reliability and accuracy of this kind of models should be evaluated with respect to a population of pumps, since referring to a single pump sample may easily lead to over/under-estimate the quality of the proposed approach. In order to achieve a complete overview of the model reliability, comparison has been also carried out with respect to the average pump, i.e. the pump in which each geometrical parameter is the mean value of the measurements performed on the 20 samples. In this case, the simulated efficiency resulted to fall within the 98% confidence interval estimated by using the Student's t-distribution for each analyzed working condition. The overall process of model validation has therefore produced satisfactory results with respect to the purposes of the model.

Finally, an analysis of the different outcomes provided by the model has been carried out, in order to underline its potentialities. Further analyses focused on addressing the influence of the speed increase on the pump behavior have enlightened the effective additional value guaranteed by studying gear pumps performance by using a multiphysical approach. In particular, the possibility to explain the correlation between the high pressure peak in the trapping zone and the sealing level reduction in the pressurizing zone underlines the capability of the proposed modeling approach to analyze the machine behavior from multiple points of view. This characteristic assumes a particular advantage in the field of gear pump performance simulation, where the overall machine behavior is the result of the mutual interaction between different phenomena arising from design aspects that may appear uncorrelated at first.

4

EXPERIMENTAL DETECTION OF CAVITATION IN EXTERNAL GEAR PUMPS BY VIBRO-ACOUSTIC MEASUREMENTS

In the present Chapter, cavitation in external gear machines is investigated by means of a dedicated experimental campaign. Four different pump prototypes have been designed and manufactured to perform this research, one of them specifically built up to not be affected by such a phenomenon. Cavitation is induced in the testing procedure by increasing the working speed, in order to better reproduce the development of the phenomenon in actual applications. Vibro-acoustic measurements performed by a hydrophone and a high-frequency accelerometer are put in comparison with measurements of inlet and outlet pressure ripple, in order to enlighten their capability to effectively provide an earlier detection of the phenomenon. Waterfall spectra are investigated and later RMS values of the filtered signals are shown with respect to the cavitation number and compared with efficiency measurements. Results demonstrate that vibro-acoustic measurements associated to a dedicated signal processing procedure represent a powerful tool to detect cavitation inception in gear pumps. Effect of oil temperature is investigated, showing that it contributes in spreading the phenomenon on a wider speed range. Finally, the comparison between different pump prototypes enlightens the capability of the presented procedure to quantitatively estimate the intensity of the cavitation phenomenon.

4.1 INTRODUCTION

Cavitation detection in fluid machinery represents a central but demanding task in defining the performances of pumps and turbines throughout a wide range of working conditions. Characterizing the machine's behavior from the

onset of the phenomenon until its full development usually requires a well-assessed measurement procedure and accurate post-processing.

One of the very first works on this subject pertains to I. S. Pearsall [10], that focused the attention on determining the effects of cavitation by means of acoustic measurements on the performance of various hydraulic machines, such as axial-flow and centrifugal pumps, as well as Francis and Kaplan turbines. Measured data demonstrated that acoustic measurements were more sensitive to the phenomenon inception than efficiency measurements. These first results have been later supported by more extended experimental campaigns performed on centrifugal pumps [11], demonstrating the effective capability to detect cavitation inception by using hydrophone sensors.

The measurement approach described in [10, 11] has been lately developed and applied to various Kaplan and Francis turbine prototypes [85, 86], underlining the chance to improve the experimental detection with blade-passage frequency demodulation techniques. Results have been then supported by other investigations also performed on pump-turbines [87] with different transducers as accelerometers and Acoustic Emission (AE) sensors [88]. More recently, different signal processing techniques have been proposed for detecting cavitation inception: M. Čudina demonstrated the possibility to characterize the phenomenon in centrifugal pumps by using audible sound [89, 90]; Adamkowski et al. focused the investigation on monitoring the pump shaft torsional vibrations induced by cavitation erosion [91]. In the same years, Zhaoli et al. presented an assessed method to detect cavitation in pumps with the help of phase demodulated ultrasonic signals [92], while Poddar and Tandon adopted acceleration and AE measurements to detect cavitation in journal bearings and proposed a physical explanation of the obtained results. Gohil et Saini evaluated the effect of temperature and other working parameters on cavitation in Francis turbines [93], while M. M. Stopa et al. demonstrated the possibility to detect the phenomenon inception in centrifugal pumps with the help of a load torque signature analysis [94].

Various other experimental studies on this challenging subject may be found in the literature, however, despite the wide interest shown by the scientific community, a lack of results concerning the detection of cavitation in volumetric machines has been observed by the authors. A small amount of research has been performed on evaluating the effects produced by air release/absorption and oil vaporization in volumetric pumps and motors. Moreover, such

works are generally restricted to the numerical approach and focused on the assessment of models for performance prediction. In particular, in [48] Borghi et al. evaluated the influence of cavitation in external gear pumps and motors by proposing a lumped parameter model restricted to the meshing zone, only. More recently, in [95, 49] Zhou et al. presented a lumped parameter approach to evaluate external gear pump performance under cavitation conditions based on simplified transport equations obtained from the full cavitation model [96]. The model described in [49] is supported by experimental data referring to the pressure ripple around gears, but no effective data regarding the cavitation detection are provided. Effects produced by cavitation in external gear pumps have also been evaluated by using 2D Computational Fluid Dynamic (CFD) approaches as the one proposed by del Campo et al. in [58, 97], where the performed simulations predicted the effects of cavitation to be restricted on the inlet flow rate/pressure ripple, exclusively. Simulated results are supported by qualitative comparison with inlet chamber streamlines detected by using Time-Resolved Particle Image Velocimetry; however, no effective detection of cavitation is performed. A similar approach has been also proposed in [98], where Liu et al. made use of a CFD analysis to evaluate cavitation effects in rotor pumps.

As far as the authors are aware of, the only one experimental work focused on cavitation monitoring in volumetric pumps pertains to Buono et al. [99], that presented an experimental campaign aiming at characterizing the phenomenon in gerotor pumps by means of pressure ripple and vibration measurements. Experimental measurements on cavitation in gear pumps cannot be found in the literature even if this machine type is commonly known to be affected by such a phenomenon [48, 49, 58, 97]. Concurrently, similar studies focused on gears, as the one described in [100], are not common. This lack of data might be justified by considering that gear pumps are traditionally driven by electric motors or low speed engine since the requested delivery flow rate is obtained by increasing the pump displacement. Nowadays, in particular in the automotive field, the need to reduce weight and dimensions of the overall system requires to reduce the pump displacement as much as possible and then to guarantee the requested delivery flow rate by increasing the working speed. Based on this brief literature review, the goal of the present Chapter is to present an extended experimental campaign focused on the vibro-acoustic characterization of the cavitation phenomenon in ex-

ternal gear pumps. Results obtained from the signal processing of different sensors such as accelerometers, hydrophone and pressure pulsation sensors are shown and discussed. Moreover, the analysis of measured data referring to different pumps is supported by measurements of volumetric efficiency and actual detection of various damages produced by cavitation.

The following section describes the characteristics of the cavitation phenomenon in fluid machines. Section 4.3 outlines the test setup, concentrating on the description of the test bench adopted to evaluate both pumps efficiency and vibro-acoustic performance, the data acquisition system together with the various transducers installed on the rig and, lastly, the four external gear pumps designed for the experimental campaign and the measurement procedure. Section 4.4 describes the signal processing techniques applied to measured data, while Section 4.5 presents the obtained results, with the aim at characterizing gear pump behavior under cavitating conditions. Finally, last section is devoted to concluding remarks.

4.2 CAVITATION IN FLUID MACHINERY

The literature review in Section 4.1 demonstrates that the cavitation phenomenon in axial/centrifugal pumps and turbines has been widely studied throughout the last five decades. Several experimental campaigns contributed in addressing its characteristics, from a machine performance point of view, as in refs. [10, 11], as well as from a physical point of view, as in ref. [87]. The former approach is based on the evaluation of the machine performance parameters, such as efficiency or emitted noise, with respect to its working condition, which is usually defined in terms of the cavitation number σ:

$$\sigma = \frac{P_{in} - P_{sat}}{0.5\rho u^2} \tag{86}$$

where P_{in} is the mean inlet pressure, P_{sat} is the saturation pressure at the reference oil temperature, ρ is the oil density at the reference temperature and u is the mean flow velocity at the inlet port. As described in ref. [101] pag. 129, the cavitation number is a scaling parameter adopted to extrapolate data from one working condition to another by assuming complete similitude guaranteed by a constant cavitation number itself. For the sake of completeness, in the same reference, it is also underlined that σ does not include all

the variables influencing the phenomenon, e.g. boundary geometry, absolute pressure, local velocity or pressure drop, and therefore such a parameter is still affected from scale effects. Once the cavitation number is assumed as a control parameter, starting from a cavitation-free working condition, by reducing σ the generic turbomachine cross three main regions: the first one coincides with the initial condition, then as the machine approaches the cavitation inception region, small, isolated and localized bubbles start appearing. As σ keeps decreasing, the phenomenon intensifies till the machine enters the fully-developed cavitation region and starts working in chocked conditions.

These considerations explain the results obtained by Pearsall and McNulty in refs. [10, 11], which demonstrated that efficiency measurements cannot follow the evolution of the phenomenon entirely, since delivery flow rate starts being influenced by cavitation just after the machine enters the fully-developed cavitation region. On the contrary, measurements based on hydrophones, accelerometers, acoustic emission sensors and pressure transducers were shown to be much more sensitive to the phenomenon, being able to detect it from the inception to its complete development. In particular, several experiments demonstrated that vibro-acoustic measured quantities always follow a common trend as the cavitation number is decreased from the free-of-cavitation region till the fully-developed one, as shown in Figure 55. Volumetric efficiency η_V remains unaltered till the chocked condition, when it finally shows a sharp drop; on the contrary, generic vibro-acoustic quantity χ starts increasing as soon as the inception takes place, reaches a maximum and then suddenly drops down as the phenomenon intensifies. If σ is further decreased, chocking starts appearing and χ starts increasing again.

These results are usually obtained by executing a large number of measurements where σ is gradually decreased by reducing the inlet pressure while the working speed is set as a constant. The practical advantage given by this kind of approach stands in the possibility to fully characterize the phenomenon by simply regulating a valve placed on the inlet side. Moreover, since this kind of machines is typically designed to work at a fixed constant speed while the inlet pressure depends on the installation layout, the proposed approach also gives an accurate representation of the real case. It is worth specifying that the correlation between the measured trends and the physical development of the phenomenon has been widely cross-checked with the help of particle image velocimetry observations (see for example refs. [87, 88, 102]).

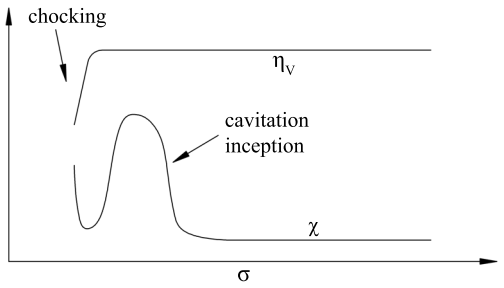

Figure 55: Qualitative trend of volumetric efficiency η_V and generic vibro-acoustic quantity χ with respect to the cavitation number.

In order to have a complete overview of the problem, it must be clarified that the necessity to detect cavitation inception comes from a practical reason. Although fully-developed cavitation affects volumetric efficiency seriously, it is proved to be less damaging than the inception condition in terms of wear and erosion. As explained in refs. [101, 103], when cavitation becomes well developed, the flow aggressiveness tends to decrease due to a smaller production of vapor bubbles or weaker implosions. For this reason, detecting cavitation from its inception become a crucial task to define the working condition range where the machine can operate safely.

Despite the large amount of specialized literature regarding cavitation on hydraulic machines, similar studies have never been performed for gear pumps. For this reason, a clear description regarding how and where the phenomenon takes place and evolves is not available in the literature. Concurrently, no experimental data for correlating cavitation in gear pumps with respect to vibro-acoustic measurements can be found. However, by analyzing the typical pressure evolution around the gears, it is possible to assume a realistic description of its development. Since bubble generation requires a consistent drop of the local pressure, air release and vaporization must necessarily take place in the meshing zone, when the trapped volume opens to the inlet chamber. Within this context, the oil suddenly moves from a high pressure zone to a low pressure one through an extremely small orifice, which causes the flow velocity to increase significantly and concurrently produces a further decrease of the local pressure. Once bubbles are generated, they can either collapse in the suction chamber or be trapped by the gear pockets which drag them into

the pressurizing zone. As soon as the pressure inside the pocket increases, the bubble collapses producing undesired noise, vibration and, potentially, wear.

On the basis of this description, both working speed and suction pressure are crucial parameters. If the speed is increased, the pressure peak inside the meshing zone increases as well and therefore the subsequent pressure drop becomes more and more intense. Moreover, the speed increase produces a slight reduction of the mean suction pressure that contributes in intensifying the phenomenon. On the other hand, cavitation can be also induced by decreasing the mean inlet pressure till bubble generation can take place directly inside the suction chamber. It is worth noting that the two mechanisms cannot be considered equivalent since the two parameters have a different influence on the pressure course around the gears. As shown in Chapter 3, in particular, the speed increase produces a consistent reduction of the pump sealing capability; since the pressure increase in the pressurizing zone is delayed, the bubble collapse is also expected to be delayed. This phenomenon is not expected if cavitation is induced by decreasing the suction pressure, because such a modification should actually improve the sealing capability of the pump by increasing the mean eccentricity between the gear shafts and the bearings.

The proposed explanation clarify the reason why cavitation tests in gear pumps for automotive applications should be performed by increasing the working speed rather than reducing the inlet pressure. This kind of pump are designed to work safely throughout an extended speed range, while the installation layout is fixed; in this way, each specific pump is designed for a specific lubrication system. For this reason, the inlet pressure does not actually represent a control parameter of the phenomenon in this particular application.

4.3 EXPERIMENTAL SETUP

4.3.1 *Test rig description*

The test rig adopted to carry out the experimental campaign is based on the same basic framework shown in Figure 34, even if it presents a completely different layout of the adopted transducers, as underlined in Figure 56. The gear pump is installed inside a sealing box that makes it working submerged and driven by a brushless AC motor with speed controller; a torque meter

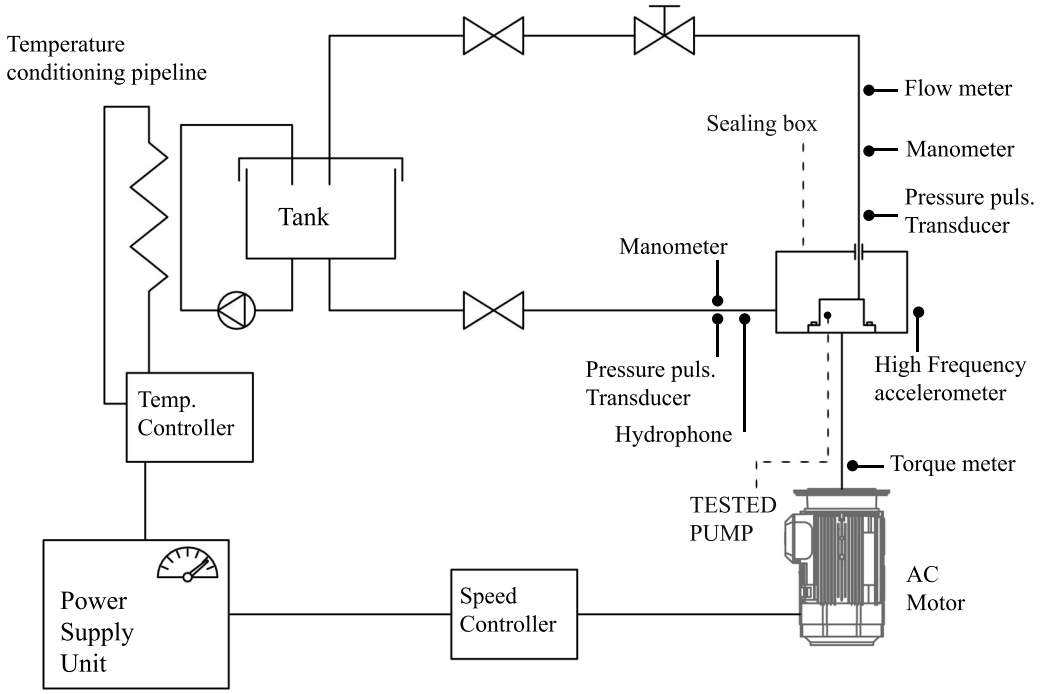

Figure 56: Test rig configuration and sensors disposition adopted for the experimental campaign.

is located along the shaft connecting the pump with the electric motor. The pipeline for the oil supply system is constituted by two branches: one connecting the tank to the sealing box and the other one connecting the pump's outlet chamber to the tank. An automatic servo valve located on the latter branch of the pipeline allows for the fast regulation of the oil delivery pressure. The oil temperature is regulated with an additional pipeline connected to the tank and controlled by a dedicated system, namely the temperature controller. Such a system monitors the oil inside the tank by using a thermocouple and regulates the temperature with a number of electric resistances.

Both pipeline systems described above are equipped with a drainage system, various valves and filters in order to allow for a safe and easy management of the test rig during the measurement procedures. The description of such auxiliary parts of the test rig is neglected being out of the scope of the present work.

4.3.2 *Sensors and data acquisition system*

Two different sets of transducers have been adopted to carry out the experimental campaign. As shown in Figure 56, a first set of sensors has been used to control the test rig and monitor the working condition of the pump under examination. In particular, two digital pressure gauges have been placed on the suction and delivery ports, respectively, in order to check the mean inlet and outlet pressure. A Kracht Gear Type Flow Meter has been placed on the delivery pipeline to measure the outlet flow rate and therefore determine the volumetric efficiency, while the instantaneous angular speed can be directly acquired from the tachometer connected to the speed controller of the electric motor. This first set of transducers is directly acquired by the data acquisition system integrated in the test bench.

The second set of sensors has been specifically designed to detect the presence of cavitation by means of vibro-acoustic measurements (see Figure 57). With this purpose, two high frequency piezoelectric transducers (model PCB S102B with resonant frequency above 500kHz) have been place on the suction and delivery ports respectively, in order to measure the pressure ripple generated by the pump. Moreover, a miniature hydrophone (model B&K 8103), located in proximity of the suction chamber and connected to a conditioning amplifier (model B&K Nexus 2692), monitors the acoustic pressure of the oil. Finally, a high-frequency single-axis accelerometer (model PCB 352A60 with resonant frequency above 95kHz) has been located on the sealing box, close to the beginning of the pressurizing zone related to the driving gear. This choice is justified by the fact that while bubbles are generated in the last part of the meshing zone, they are supposed to collapse in the first part of the pressurizing zone. This assumption is supported by direct observation of the wear produced by cavitation on the pump casing and it will be better described in the following subsection. This second set of sensors, together with the signal provided by the tachometer, has been acquired with a LMS Scadas 305 acquisition system and then postprocessed in Matlab environment. In order to capture the signature produced by cavitation phenomena, the sample frequency f_s has been set to the maximum value allowed by the adopted acquisition system, which is equal to 204800Hz.

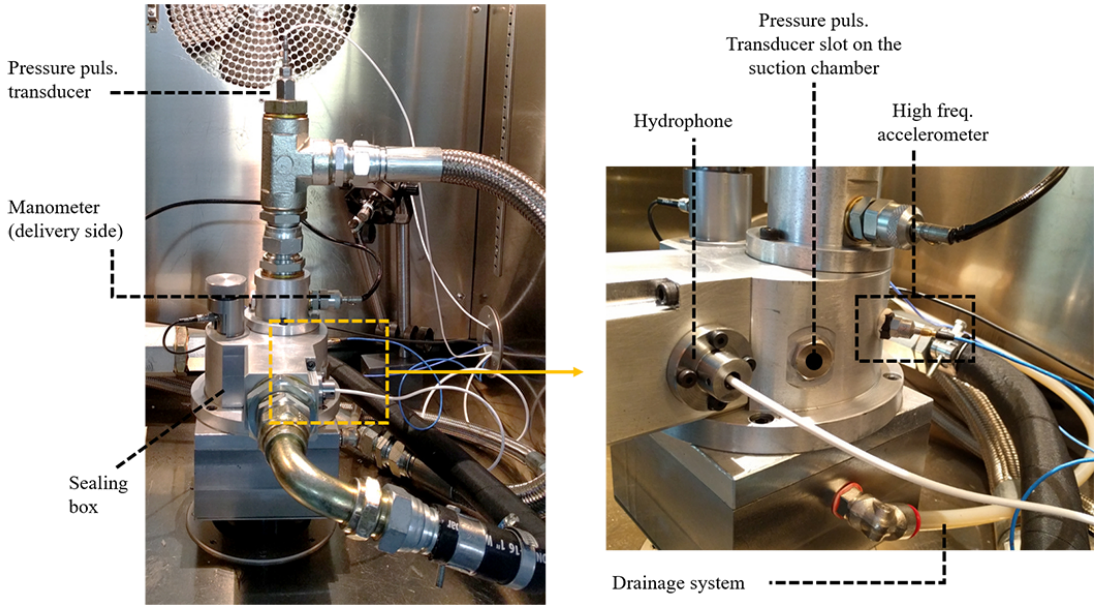

Figure 57: Transducers setup in the real test configuration. As underlined in Section 4.3.1, the sealing box does not allow for a direct access to the pump casing.

4.3.3 *Gear pumps type and measurement procedure*

Four different gear pump prototypes have been designed and manufactured in order to perform a wide experimental campaign allowing for a satisfactory characterization of the phenomenon. The first prototype, namely Pump A, is constituted by helical gears, with 14 teeth on the driving gear and 9 teeth on the driven one. Since the pump casing is made by steel, no running in process is required and therefore radial clearances between gears and casing are entirely defined by design. The second prototype, namely Pump B, is composed by the same gearpair used for Pump A, but the casing is milled from a single block of aluminum. For this reason, radial clearances are reduced during the design process since the gear pair can mill its own grooves into the casing during the running in process. The third prototype, namely Pump C, is made up by a spur gearpair, with 13 teeth on the driving gear and 10 teeth on the driven one. As described for Pump B, Pump C has an aluminum casing that requires the running in process before the pump can be considered ready to be tested. Finally, the last prototype, namely Pump D, is made

Table 12: Main design characteristics of the four tested prototypes.

Pump Type	z_1/z_2	**Tooth Type**	**Case Material**	P_{out}
A	14/9	Helical	Cast iron	30bar
B	14/9	Helical	Aluminum	30bar
C	13/10	Spur	Aluminum	30bar
D	11/11	Helical	Aluminum	30bar

by an aluminum casing and helical gears, with 11 teeth and transmission ratio equal to one. All the four prototypes have similar global dimensions and displacement (around $14cm^3/rev$). Pump D has been specifically designed to avoid the presence of cavitation inside the range of working conditions tested. The main design features of the four described prototypes are summarized in Table 12.

The four pumps have been tested by following the same measurement procedure: the prototype is installed on the test rig and the servo valve is set to maintain a mean delivery pressure equal to 30bar. The oil temperature is set at 60°C and kept as a constant by the temperature controller. With these constraints settled up, each pump is tested at different speed values, starting from 800rpm till 6000rpm, with a constant step of 100rpm. The maximum speed is limited by the maximum torque provided by the electric motor. Moreover, experimental tests regarding prototype A have been repeated at 90°C and 120°C in order to evaluate the influence of the oil temperature. Tests have been performed without reducing the inlet pressure by regulating a valve in the inlet piping, but the speed increasing solely induces cavitation. Despite this testing procedure is uncommon when evaluating the influence of cavitation in fluid machines, it is a more realistic representation of the phenomenon that may take place in actual gear pump applications, e.g. in the auxiliary systems for automotive applications. These pumps are usually driven by the engine and therefore must properly work throughout a wide speed range; on the contrary, the installation can be designed to minimize pressure losses on the inlet pipeline making this parameter less dominant on the evolution of the phenomenon.

In order to verify the presence/absence of cavitation in each pump prototype, endurance tests have been performed on each gear machine and later the

potential presence of wear has been assessed. Endurance tests have been performed for 60 hours at the most severe working condition, which corresponds to a combination of angular speed/delivery pressure equals to $6000 rpm/30 bar$. As expected, wear has not been detected on pump prototype D, while various marks of erosion due to cavitation have been observed on prototype A, B and C. In particular, endurance tests on various samples of pump prototype A had to be stopped before the expected time due to severe wear that compromised the correct machine operation. Figure 58 shows an example of the damages produced by cavitation on the pump body and thrustplate of prototype B. As it can be noticed, cavitation caused erosion of the pump body at the suction side of the pressurizing zone, on both the driving gear bore (Figure 58.a) and the driven gear one (Figure 58.b); moreover, wear is also present on driven gear side of the thrust plate (Figure 58.c). Similar damages have been observed on pump prototypes A and C as well and the repeatability of such results has been checked by reproducing the tests on different samples of the same prototypes. Efficiency measurements have been also conducted to double-check the effective presence/absence of cavitation on each prototype by verifying the presence/absence of efficiency drops in the speed range where the phenomenon is supposed to occur; results will be shown in Section 4.5.

4.4 POST PROCESSING

The early detection of cavitation phenomena in fluid machinery by means of vibrational and acoustic measurements requires the design of specific post processing procedures, typically based on the evaluation of the demodulated signal at the blade passage frequency [85, 86, 87, 88]. However, the application of these methods in the present study did not provide any valuable result. It is the author's belief that such a negative outcome is linked to the methodology adopted in this study to promote cavitation, which is induced by increasing the working speed of the pump, without modifying any other working condition parameter. This method differs considerably from the classical approach that has been described in the literature since the very first publications, in which cavitation is promoted by reducing the suction pressure at constant nominal speed. This latter method has the benefit to freeze the dynamics of the machine with respect to the working condition; as a consequence, any

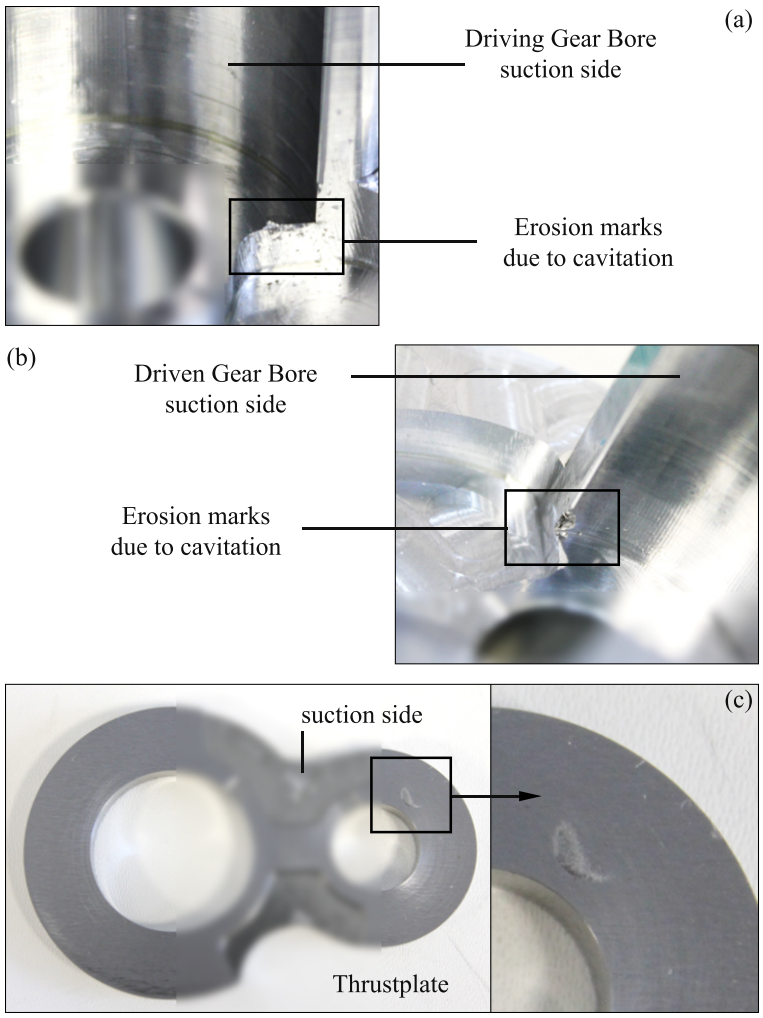

Figure 58: Examples of erosion marks due to cavitation detected on prototype B after endurance test. Damages are localized in the suction side of the pressurizing zone, both on the driving gear bore (a) and driven gear one (b), as well as on the thrustplate (c). Parts of the pump are blurred for confidentiality reasons.

change recorded in the machine response can be attributed to the cavitation development. Concurrently, as explained in Section 4.2, the approach is a well representation of real cases: this kind of axial/centrifugal machines are designed to work at fixed nominal speed, but may encounter different suction pressure values depending on the installation layout. On the contrary, gear

pumps for automotive applications are designed to be installed on a specific layout, i.e. a specific driveline transmission, but they are required to work safely throughout a wide speed range. Within this framework, it is therefore clear that promoting cavitation by increasing the working speed is a more realistic reproduction of the real case, even if the machine dynamics becomes to be influenced by both the working condition and the cavitation development. As a matter of fact, the speed increase causes the amplitude of the harmonics of the mesh frequency, together with their sidebands potentially present, to vary through the considered speed range depending on (i) the dynamics of the gearpair, (ii) the dynamics of the overall pump body and (iii) the fluid-dynamics of the machine. This particular behavior masks the signature of cavitation throughout the low frequency range typically excited by the first $10 - 15$ harmonics of the mesh frequency.

On the basis of these considerations, the phenomenon has been characterized by using an energetic approach applied to a frequency range less involved by the pump dynamics. The first step of the developed procedure consists of calculating the waterfall diagrams of the acquired signals. Waterfall charts are not determined by performing a Short Time Fourier Transform on a single run up, since they can be directly estimated by piling the data acquired at constant speed and expressed in frequency domain on a single chart. By repeating this procedure for each sensor, a general overview of the pump behavior is obtained and the frequency limit value that bounds the low frequency range can be defined by direct observation of such charts. Moreover, as it will be shown in Section 4.5, waterfall diagrams allow for a preliminary and qualitative evaluation of the presence of cavitation.

The second step of the post processing procedure starts with filtering the data by using a high-pass filter with cutoff frequency equals to the frequency limit value determined in the previous step. Filtered signals at each working speed are then analyzed by calculating their RMS value and displayed with respect to cavitation number σ [11]. The methodology is able to determine the presence of high frequency cavitation noise, in particular when enlightened by the presence of resonances inside the analyzed frequency range. However, since it may be difficult to identify the cavitation noise from structural noise, the procedure needs to be assessed by applying it to noncavitating pumps.

4.5 RESULTS AND DISCUSSION

In the current section, results obtained from the signal processing procedure described in Section 4.4 are shown and discussed. Attention is particularly focused on showing the signature caused by the presence of cavitation and the different capability of the four adopted sensors in capturing the phenomenon.

In order to better understand the importance of the first step of the post processing procedure, waterfall charts of the signals referred to pumps B and D are reported in Figure 59. It is worth reminding that the latter is specifically designed to not be affected by cavitation in the analyzed working range conditions. Results, that are displayed in logarithmic scale, have been previously normalized by their maximum value and divided by the reference value $k = 10^{-3}$ (the normalized quantity is indicated with symbol $\tilde{X}$). For each plot, two main regions can be distinguished: the low frequency region, which extends to the 40kHz limit in the currently analyzed pumps, and the high frequency region, which involves the remaining frequency range. The former region is mainly influenced by the periodic components of the signal, typically harmonics of the angular speed and the mesh frequency. The latter, on the contrary, refers to a frequency range that is usually too high to be crossed by harmonics of the mesh frequency with a relevant amplitude. Concurrently, as also observed in [11, 85, 87], the high frequency range is usually the one characterized by the cavitation signature. Based on these considerations, the waterfall plots become a powerful tool for the determination of the frequency limit that will be used to set the cutoff frequency of the high-pass filter in the following step of the post processing.

Waterfall charts in Figure 59 represent also a valuable tool for a preliminary detection of cavitation. Focusing the attention on the suction chamber pressure ripple, for example, the signals referred to the two pumps show a completely different behavior in the high frequency region. For each arbitrary frequency band within this region, the noncavitating one (prototype D) is characterized by the absence of amplitude gradient along the entire speed range, except for the presence of some high order harmonics of the mesh frequency. On the contrary, the signal referred to the cavitating one (prototype B) outlines the presence of high frequency broadband components between 40 and 70kHz. Such broadband components start being appreciable, in terms of amplitude, qualitatively from 4200rpm, reach a maximum amplitude value at

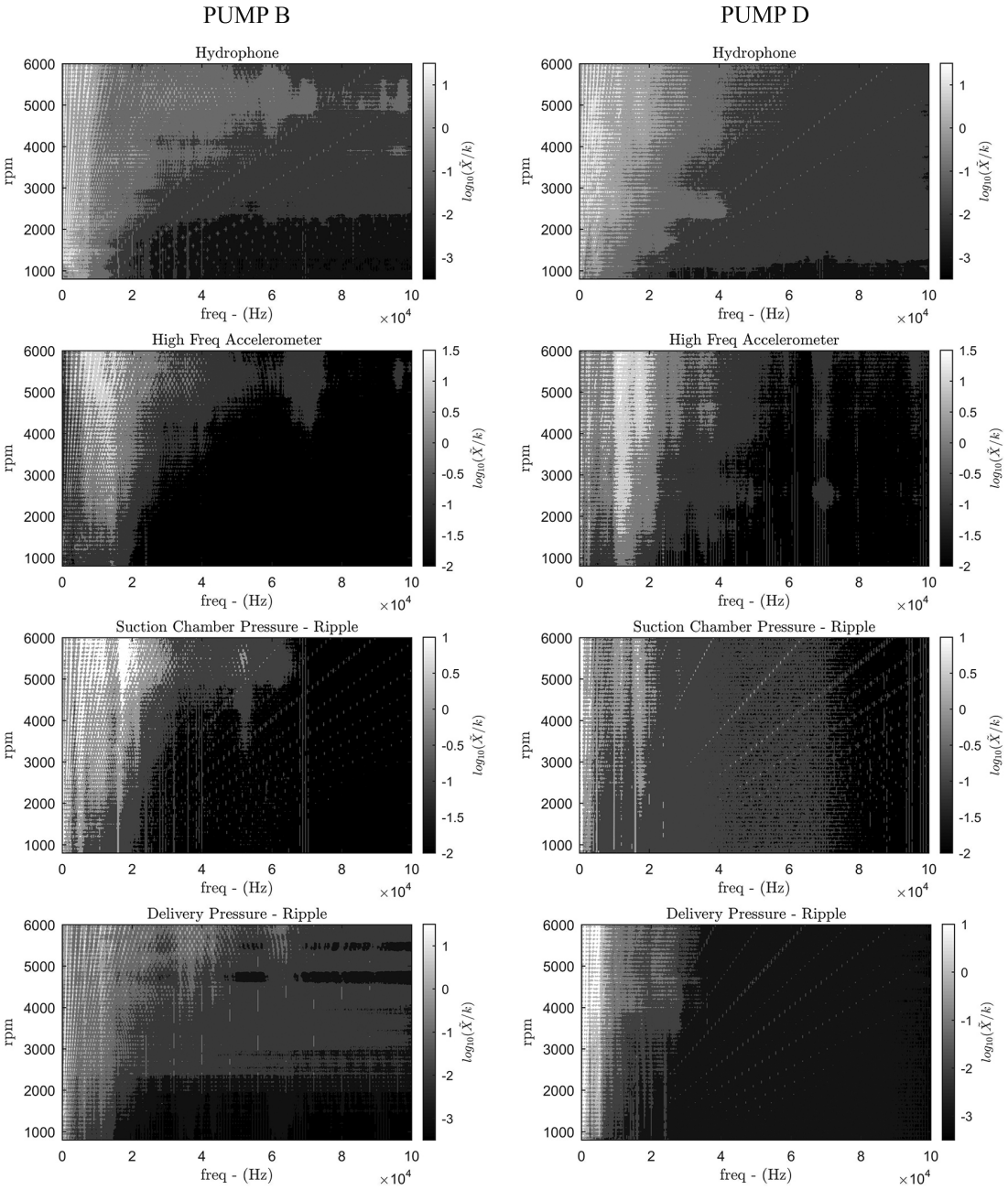

Figure 59: Waterfall plots (in logarithmic scale) of the acquired data referred to pump prototype B, affected by cavitation, and prototype D, not affected by cavitation. In each plot, symbol $\tilde{X}$ refers to the measured quantity normalized by its maximum value.

around 5500rpm and then a decrease is observed. The described phenomenon is recognized also in the signals obtained from the other transducers; in particular, hydrophone measurements appear to be the most sensitive, since such a behavior is present throughout the entire bandwidth of the high frequency region.

By following the signal processing procedure defined in Section 4.4, data referred to pump prototypes B and D have been high-pass filtered at 40kHz and then the RMS value for each transducer at each working speed condition has been calculated (Figure 60). Results are reported together with the measured volumetric efficiency and expressed with respect to the cavitation number σ. For the sake of clarity, measurements performed with hydrophone, accelerometers and pressure transducers are normalized by their respective minimum value. Volumetric efficiency is normalized with respect to its maximum value for confidentiality reasons. As it can be appreciated from Figure 60, the efficiency referred to pump B shows the typical sharp drop caused by the presence of intense cavitation; on the contrary, no efficiency reduction is detected for pump D. By focusing the attention on the cavitating one, it is possible to observe that in conformity with the efficiency drop that starts taking place at about $\sigma = 5$, all the four signals show a strong increment of the RMS value. Moreover, as often described in the literature [10, 11, 88, 89], the RMS value reaches a maximum when cavitation is close to the fully developed condition and then starts decreasing. It is therefore clear that intense cavitation phenomena are captured by pressure pulsation measurements as well as acceleration and acoustic measurements. However, since it is well known that incipient cavitation takes place well before the efficiency drop [10, 11, 88], it is interesting to notice that pressure pulsation measurements appear not to be able to detect it. In particular, suction chamber pressure pulsation results to be the least sensitive to the phenomenon since the RMS value begins to increase when the efficiency drop is already developed. On the contrary, both acceleration and acoustic measurements start rising considerably before the efficiency drop, and in particular around $\sigma = 15$. In analogy to the observations made in [88], it is reasonable to assume that incipient cavitation takes place in the range between $\sigma = 10$ and $\sigma = 15$, where pressure pulsation measurements are not affected by a significant variation in their RMS values.

The behavior described by vibration and acoustic measurements can be also appreciated in Figure 61, which reports the results of the post processing

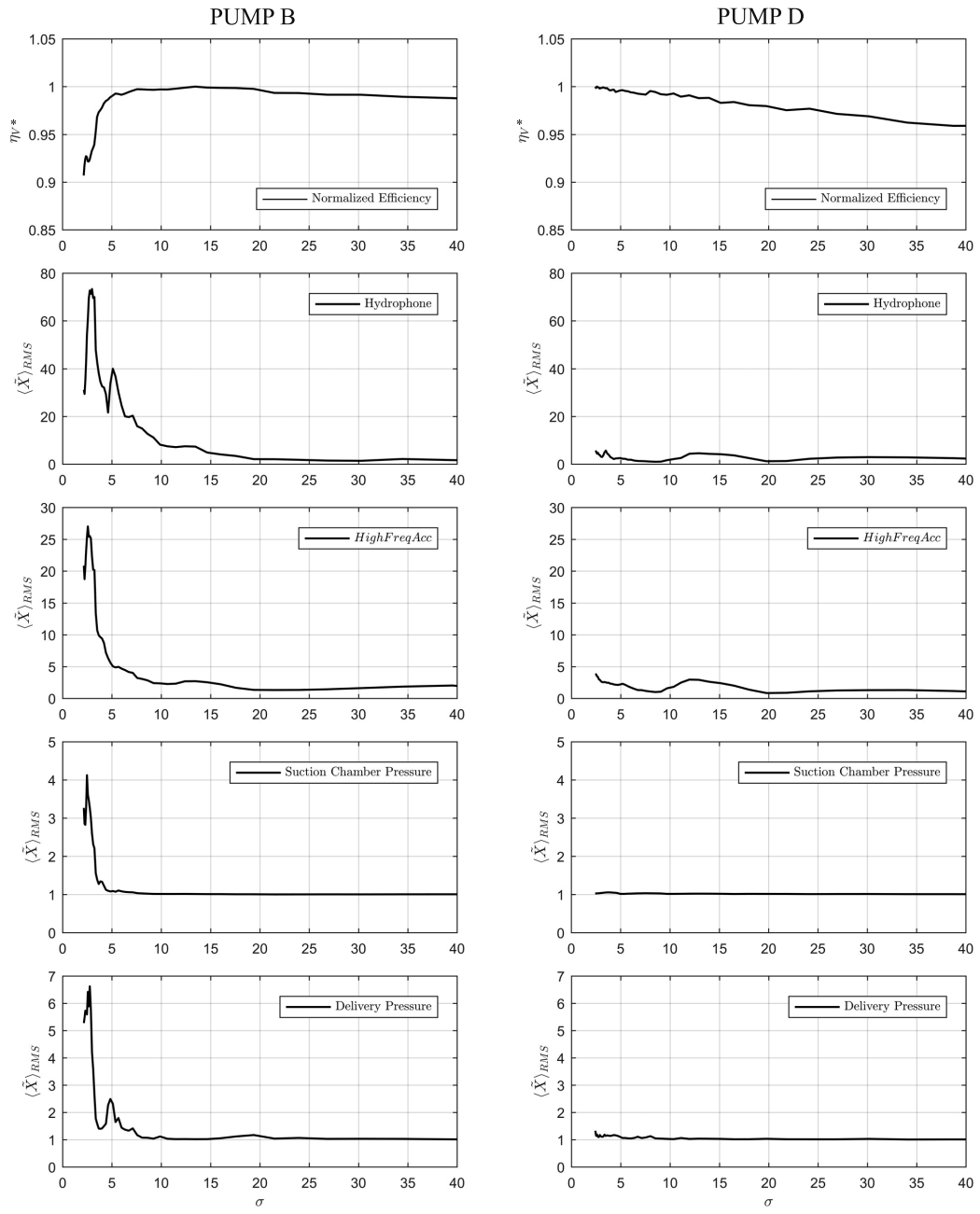

Figure 60: RMS values of the four measured signals and volumetric efficiency as a function of the cavitation number σ, for pump prototypes B and D. In each plot, symbol $\tilde{X}$ refers to the measured quantity normalized by its minimum value.

applied to acoustic measurements performed on prototype A at three different temperature values. The cutoff frequency of the high-pass filter has been set at 45kHz and results have been normalized by the minimum value obtained for the 60°C case. By focusing the attention on the 60°C case, it can be noted that the analyzed speed range (from 800rpm to 6000rpm) is able to characterize the entire development of the phenomenon, which starts being detected at $\sigma = 14$. By increasing the speed, i.e. by reducing the cavitation number, RMS value increases and reaches a maximum at $\sigma = 3.10$; after this value, the RMS of the filtered signal shows a sharp drop till the minimum value recorded at $\sigma = 2.38$ and it then starts raising again. Such a particular behavior has been described several times in the literature for rotordynamic machines [10, 11, 88, 89, 90] but no similar data are already available in the literature for positive-displacement machines. Figure 61 allows also for the evaluation of the effect produced by the oil temperature on the cavitation phenomenon. As it can be appreciated, temperature variation does not cause a significant modification of the overall behavior since the maximum of each curve is bounded by $\sigma = 2.97$ and $\sigma = 3.43$. However, since for a given working speed the temperature increasing makes the cavitation number to reduce, measurements performed at 90°C and 120°C cannot describe the development of the phenomenon entirely. Practically speaking, the increase of oil temperature spreads the phenomenon on a wider speed range and, in particular, it moves the fully developed cavitation condition at higher speed values.

The comparison between pump prototypes A and B allows for the evaluation of the effects related to the choice of a different casing technology. As described in Section 4.3.3, pump A has been designed with a cast iron casing that does not require running in processes; this means that radial clearances are entirely defined during the design procedure. On the contrary, prototype B is constituted by an aluminum casing, which undergoes a dedicated running in process allowing for the gearpair to produce a certain amount of wear and therefore modify the radial clearances by itself. Apart from this aspect, the two pumps are identical. On the basis of these considerations, Figure 62 shows the comparison between the two pumps in terms of the vibro-acoustic response, normalized with respect to the minimum value calculated for pump prototype A; measured efficiency is given as standard proof of the presence of cavitation. Although the overall behavior is similar, RMS values referred to pump B are considerably smaller in the range where the cavitation takes place; on

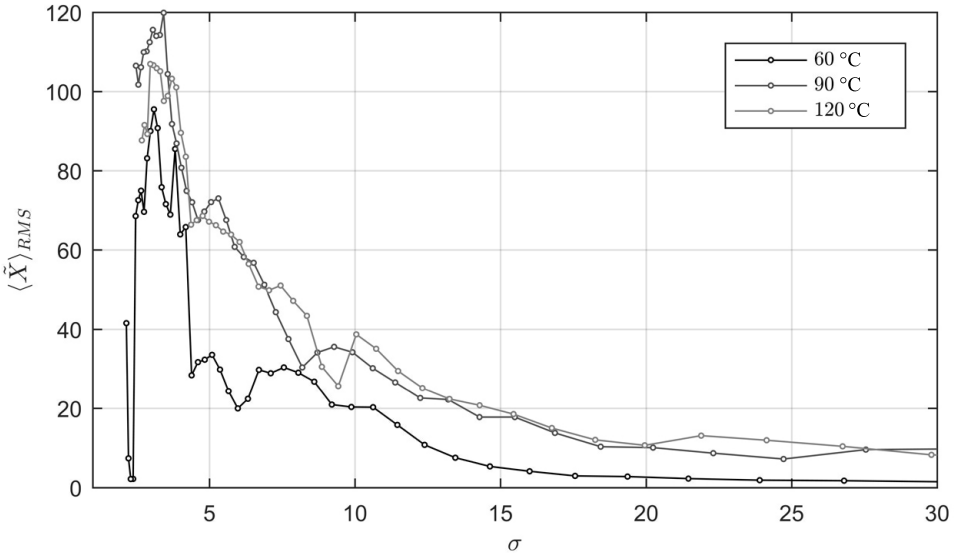

Figure 61: RMS values referred to the hydrophone measurements on pump prototype A at different oil temperature. Symbol $\tilde{X}$ refers to the measured quantity normalized by the minimum value recorded for the 60°C case.

the contrary, outside this range, calculated values are similar both regarding acoustic and acceleration measurements. It is therefore reasonable to assume that, since the running in process permits the gearpair to self-adjust its radial clearances through a controlled wear, it also actively contributes in reducing the intensity of the cavitation phenomenon. As underlined in Section 4.3.3, the higher intensity of cavitation in pump prototype A is also proved by the presence of an excessive amount of wear observed by performing endurance tests on various samples of such a prototype. From these considerations, it results that vibro-acoustic measurements performed on external gear pumps are able to quantitatively define the intensity of the cavitation phenomenon, in addition to their capability to detect it in advance with respect to pressure ripple and efficiency measurements.

Finally, in order to assess the general applicability of the presented method, Figure 63 depicts the RMS values referred to the measurements performed with the hydrophone and the high frequency accelerometer on pump prototype C, which is made by spur gears. The cutoff frequency of the high-pass filter has been set at 45kHz. As it can be observed, the recorded behavior is

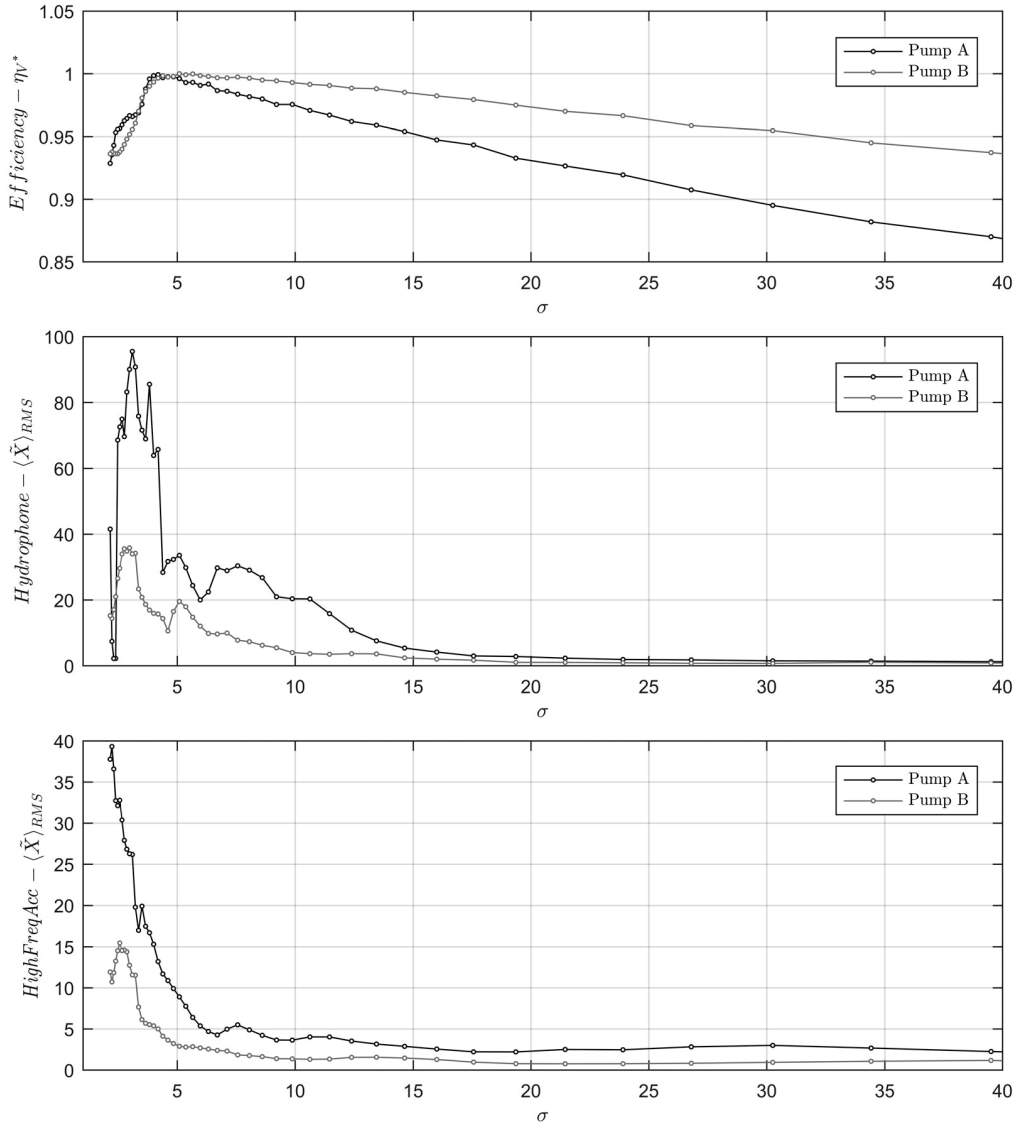

Figure 62: Comparison between pump prototypes A and B in terms of hydrophone and accelerometer response (RMS values); efficiency measurements are shown as a benchmark indicator. In each plot, symbol $\tilde{X}$ refers to the measured quantity normalized by its minimum value recorded for pump prototype A.

qualitatively identical to the one observed for pump prototype B and A: while the efficiency curve shows a sharp drop at about $\sigma = 3.8$, both acoustic and vibrational measurements anticipate the prediction. In particular, as already appreciated from Figure 60 and Figure 62, hydrophone measurements result to be the most sensitive in detecting the phenomenon.

4.6 CONCLUDING REMARKS

An extended experimental campaign aiming to detect cavitation in external gear pumps by means of acceleration and acoustic measurements has been presented. With this purpose, a dedicated test rig has been instrumented with a hydrophone and a high frequency accelerometer, together with pressure ripple transducers located both on the suction and delivery chambers. Moreover, a flow meter, a tachometer and two digital pressure gauges complete the set of transducers adopted to control the pump working conditions.

In order to perform the present study, four different pump prototypes have been designed with the purpose to evaluate the phenomenon under the effects of different design solutions. Moreover, last prototype has been specifically designed to not be affected by cavitation throughout the entire working conditions range examined; this characteristic makes it as the reference point to assess the results. The effective presence/absence of cavitation in the four prototypes has been checked with the help of efficiency measurements and endurance tests, showing examples of various cavitation erosion marks observed.

The application of the post processing procedure has underlined the necessity of a general overview of the signals, which is achieved with the help of waterfall spectra extended to the entire measured frequency range. This first step identifies two different regions: the low frequency one, which is mainly influenced by the mesh frequency and its harmonics, and the high frequency one, which is mainly characterized by the wideband cavitation noise.

Experimental data are filtered to enlighten the high frequency region and then RMS values of such signals are plotted with respect to the cavitation number. Comparison between pump B (cavitating) and D (not cavitating) has underlined the effective capability of the procedure in detecting the presence of the phenomenon. In particular, acceleration and acoustic measurements appeared to be highly sensitive to the phenomenon if compared to efficiency

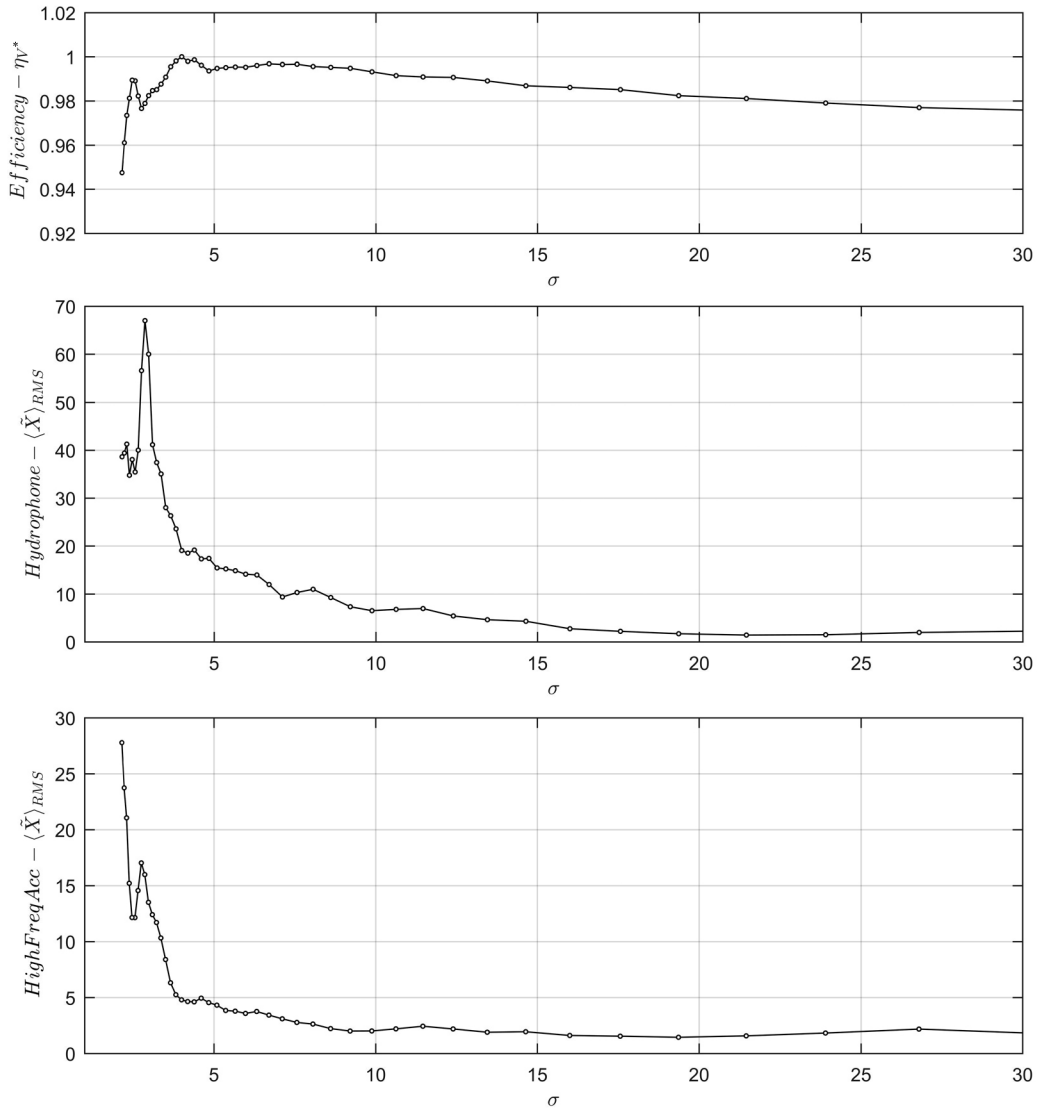

Figure 63: RMS values calculated from acoustic and acceleration measurements of prototype C; efficiency curve is shown as a benchmark indicator of the cavitation development. In each plot, symbol $\tilde{X}$ refers to the measured quantity normalized by its minimum value.

measurements as well as pressure ripple measurements. All the calculated results qualitatively reproduce the behavior usually detected in rotordynamic pumps and turbines, demonstrating that the cavitation phenomenon can be analyzed also in volumetric pumps in a similar manner. Results obtained on pump prototypes A and C (both cavitating) confirm these observations.

Influence of the oil temperature has been evaluated by reproducing the tests at three different temperature values: 60°C, 90°C and 120°C. Results seem demonstrating that the temperature increasing tends to spread the development of cavitation throughout a wider speed range and, in particular, to move the fully developed cavitation condition at higher speed values. Moreover, influence of the casing technology has been evaluated: pumps made by aluminum casings resulted to be less affected by cavitation. This result may be explained by considering that aluminum casings require the pumps to undergo a dedicated running in process that allows the gearpair to self-adjust its radial clearances through a controlled wear process. This aspect seems to contribute in reducing the intensity of the cavitation phenomenon, as verified by endurance tests performed on various samples of pump prototypes A and B. The capability of the proposed procedure to capture the intensity of the phenomenon, a characteristic that efficiency curves cannot detect, can be clearly appreciated by comparing the maximum RMS values calculated for the two pump prototypes. As a consequence of this assessment, the method resulted to be able to evaluate the severity of the cavitation in gear pumps.

The proposed study therefore demonstrates that vibro-acoustic measurements coupled with a dedicated signal processing procedure are a powerful tool for the early detection of cavitation in external gear pumps and a quantitative estimation of the intensity of the phenomenon. However, it also underlines that such a phenomenon is still not completely addressed and further studies should be devoted to analyze the nature of cavitation in gear pumps in correlation with the nature of the produced signals.

5

CONCLUDING REMARKS

The thesis addresses numerical and experimental methodologies for studying the performance of gear pumps, by taking into account the critical aspects (weight and size reduction, NVH improvements, helix influence, etc) that come out in current automotive applications. As a matter of fact, the availability of advanced methods for predicting or experimentally analyzing the pump behavior allows to reduce costs and time required by a new design project thanks to the possibility to accelerate the convergence of iterative design procedures usually based on trial and error. On the basis of these considerations, the goal of the present thesis is to provide and discuss a set of advanced tools to assist designers along the steps of the design process. For this reason, such tools are introduced by following an ideal design course starting from the analyses that can be performed at the very beginning of this procedure till the last experimental tests. Each proposed approach is focused on evaluating the machine performance from a different perspective, e.g. gearpair dynamics and machine cavitation, since modern volumetric pumps must match heterogeneous requirements simultaneously.

Chapter 2, in particular, introduces a 6 degrees of freedom non-linear dynamic model for studying the effects of different design parameters on the dynamic behavior of gear pumps, focusing attention on a wide working speed interval. The developed model is based on a simplified approach which becomes powerful at the early stages of the design process, when the detailed pump geometry is not completely defined. In this context, where the entire machine geometry usually required to run high-accuracy simulation is not available, the model estimates pressure loads by means of an analytical approach accounting for various influencing parameters such as pressurizing

zone extension, outlet pressure and potential presence of high pressure phenomena in the trapping volume, as well as the presence of speed dependent drag torque. A parametric study has been conducted in order to evaluate the effects produced by different outlet pressures, presence of speed dependent high pressure peaks in the trapping volume and various pressurizing zone extensions. Results have shown that the pressure value reached inside the trapping zone has a deep influence on the dynamic behavior of the pump, in particular in the high speed range, where the fifth natural mode can be excited by low order harmonics of mesh frequency. The analysis of the results underlines the capability of the proposed model to capture the fundamental characteristics of the pump dynamics, despite the limited amount of required parameters. Concurrently, the model enlightens the presence of deep correlations between the pump NVH characteristics and design aspects typically devoted to improve the pump efficiency and reliability.

Chapter 3 addresses the mathematical bases and the features of a numerical model for the high accuracy prediction of gear pump performance, in terms of volumetric efficiency, pressure phenomena and bearing reaction. The model is intended as a tool to assist designers at advanced stages of the design process; for this reason, the basic aim of the model is to provide a detailed and reliable description of the pump behavior in reference to its specific design characteristics. In addition, in order to ensure the wide applicability of the model in modern design solutions, possibility to study both spur and helical gears, as well as non-unitary transmission ratio gearpairs has been included. The quality of the estimation is also due to the adoption of a dedicated analytical methodology for the calculation of pressure forces and torques in both spur and helical gear pumps; such a method consists in a systematic and general procedure to consider the major number of phenomena that characterize the meshing evolution. The accuracy of this method has been discussed by comparing it with other methodologies available in the literature: results underlines the capability of the proposed procedure to determine pressure force and torque on the basis of a major number of phenomena occurring inside the meshing zone, leading to more accurate estimations. The proposed methodology itself can represent a useful stand-alone tool to precisely estimate one of the main excitation sources that contribute to define the dynamic behavior of these machines.

In order to address accuracy and reliability of the proposed lumped parameter approach, an extended experimental campaign has been carried out on a gear pump designed for automotive applications. The pump design has been reproduced in 20 nominally identical samples, in order to have a statistical characterization of the pump behavior. In addition, tooth tip/case clearances and journal bearing radial clearances have been measured on each sample, with the aim to obtain a more clear definition of their actual geometry. Results obtained from the experimental campaign demonstrate that radial clearances measured at the end of the production process may show high value of the estimated standard deviation, even if such values stand within the design tolerance interval. Moreover, although design limitations are satisfied, slight modifications of the radial clearances may consistently affect the pump performance. Such a phenomenon is amplified as the temperature increases.

Experimental data have been finally adopted to set up the lumped parameter model and perform a comparison based on the volumetric efficiency, showing that the model reaches different levels of accuracy depending on the analyzed working condition. However, in terms of delivery pressure dependence, model accuracy is always kept below the 4% limit, while the minimum value is well below the 1% limit. Concurrently, in terms of angular speed dependence, model accuracy is always kept below the 4% limit, except for the 500rpm/30bar condition, in which the mean error reaches almost the 10%. On the other hand, the minimum value is particularly satisfactory, being always less than 0.5%. In order to achieve a complete overview of the model reliability, comparison has been also carried out with respect to the average pump, i.e. the pump in which each geometrical parameter is the mean value of the measurements performed on the 20 samples. In this case, the simulated efficiency resulted to fall within the 98% confidence interval estimated by using the Student's t-distribution. The overall process of model validation has therefore produced satisfactory results with respect to the purposes of the model. Further analyses focused on addressing the influence of the speed increase on the pump behavior have enlightened the effective additional value guaranteed by studying gear pumps performance by using a multiphysical approach. In particular, the possibility to explain the correlation between high pressure peaks in the trapping zone and sealing capability reduction in the pressurizing zone underlines the potentialities of the proposed modeling approach, which allows to analyze the machine behavior from multiple points of view.

Finally, Chapter 4 deals with the description of an experimental technique for detecting incipient cavitation in external gear pumps by means of acceleration and acoustic measurements. With this purpose, the test rig has been instrumented with a dedicated set of transducers, constituted by a hydrophone and a high frequency accelerometer, together with pressure ripple transducers located both on the suction and delivery chambers. Tests have been performed on 4 different pump prototypes, with one of them specifically designed to represent the reference benchmark by being not affected by cavitation throughout the entire working conditions range examined. The application of the post processing procedure has underlined the necessity of a general overview of the signals, which is achieved with the help of waterfall spectra extended to the entire measured frequency range. This first step identifies two different regions: the low frequency one, which is mainly influenced by the mesh frequency and its harmonics, and the high frequency one, which is mainly characterized by the wideband cavitation noise. Experimental data are filtered to enlighten the high frequency region and then RMS values of such signals are plotted with respect to the cavitation number. Comparison between cavitating and not-cavitating pumps has underlined the effective capability of the procedure in detecting the presence of the phenomenon. In particular, acceleration and acoustic measurements appeared to be highly sensitive to the phenomenon if compared to efficiency measurements as well as pressure ripple measurements.

The methodologies introduced and discussed in the present thesis involve various original aspects with practical implications in the development of modern and advanced design procedures. In particular, the model described in Chapter 2 represents a fast approach to estimate the dynamic behavior of gear pumps based on a limited number of design parameters. These features make it a powerful tool at the early stage of the design process, when the detailed pump geometry is still to be defined. Within this framework, the possibility to estimate the impact of design choices on its NVH behavior by using a reduced number of design parameters constitute a novel approach in this field, where the study of the machine dynamics has been neglected for years, since designers were much more interested in taking care of the pump efficiency rather than of its vibro-acoustic performance. In addition, the analyzed results have underlined the presence of a strong correlation between basic design choices and the machine dynamics This aspect enlightens the

necessity of further studies focused on addressing the concurrent influence of relief groove shape and dimensions, radial clearances and bearings on both the dynamic and fluid-dynamic behavior of these machines. The importance of evaluating the fluid-dynamic performance in reference to the gearpair motions is farther put in evidence by the analysis of the results provided by the model described in Chapter 3. Such a model couples the effects produced by the fluid-dynamic field and the gearpair micromotions on the basis of a novel set of equations. In this context, the two phenomena are reciprocally solved, at each time-step, to obtain an accurate estimation of the machine behavior, which is reached by taking into account multiple load sources such as the presence of speed dependent friction torque. Moreover, the possibility to include the presence of helical gears and non-unitary transmission ratio gearpairs in the analysis is an original feature, which extends considerably the practical applicability of the model. Within this framework, the analytical procedure for the estimation of variable pressure loads contains different level of originality, from the possibility to calculate all the spacial components of the loads applied to helical gear pumps, to the capability to include a larger number of phenomena occurring inside the pressurizing zone in comparison to the methods already introduced in the literature. In addition, it is worth noting that, despite lumped parameter approaches are widely adopted to study gear pumps, an effective validation of the proposed approaches, based on a large number of samples and a precise estimation of the pump geometry, is not available in the specialized literature. Despite the clear advantage given by the availability of reliable numerical models, the design process still requires the definition of experimental techniques for rating real pump prototypes. This aspect become particularly essential in the assessment of cavitation, a physical phenomenon in which numerical results are still not so reliable or extremely complex to be validated. In this context, Chapter 4 provides an experimental description of cavitation in gear pumps and a valuable technique for its practical detection. Concurrently, the study also underlines the necessity of further investigations on this subject, which has never been experimentally addressed in the literature, for a deeper understanding of its characteristics and the development of more advanced monitoring procedures. Thus, the experimental and numerical techniques defined and discussed in the present thesis constitute an advanced set of tools for improving the design process, from the first geometry definition to the last design improvements.

BIBLIOGRAPHY

[1] A. Diez-Ibarbia, M. Battarra, J. Palenzuela, G. Cervantes, S. Walsh, M. De-la Cruz, S. Theodossiades, and L. Gagliardini. "Comparison between transfer path analysis methods on an electric vehicle." In: *Applied Acoustics* 118 (2017), pp. 83–101. DOI: 10.1016/j.apacoust.2016.11.015.

[2] M. Battarra, E. Mucchi, and G. Dalpiaz. "A model for the estimation of pressure ripple in tandem gear pumps." In: *ASME IDETC/CIE*. 2015, V010T11A018; 9 pages. DOI: 10.1115/DETC2015-46338.

[3] M. Battarra and E. Mucchi. "A method for variable pressure load estimation in spur and helical gear pumps." In: *Mechanical Systems and Signal Processing* 76-77 (2016), pp. 265–282. DOI: 10.1016/j.ymssp.2016.02.020.

[4] M. Battarra and E. Mucchi. "Evaluating time dependent pressure forces and torques in external gear machines by means of an analytical approach." In: *Internoise 2017*. Honk Kong, 2017, pp. 6737–6748.

[5] M. Buzzoni, M. Battarra, E. Mucchi, and G. Dalpiaz. "Noise and vibration improvements in vibratory feeders by analytical models and experimental analysis." In: *Internoise 2017*. Honk Kong, 2017, pp. 6749–6759.

[6] M. Buzzoni, M. Battarra, E. Mucchi, and G. Dalpiaz. "Motion analysis of a linear vibratory feeder : Dynamic modeling and experimental verification." In: *Mechanism and Machine Theory* 114 (2017), pp. 98–110. DOI: 10.1016/j.mechmachtheory.2017.04.006.

[7] C. Bonacini. "Sulla portata delle pompe a ingranaggi." In: *L'ingegnere* 9 (1961).

[8] H. Yanada, T. Ichikawa, and Y. Itsuji. "Study of the trapping of fluid in a gear pump." In: *Proceedings of the Institution of Mechanical Engineers. Part A: Power and process engineering* 201.1 (1987), pp. 39–45.

[9] M. Eaton, P. S. Keogh, and K. A. Edge. "The modelling, prediction, and experimental evaluation of gear pump meshing pressures with particular reference to aero-engine fuel pumps." In: *Proceedings of the Institution of Mechanical Engineers, Part I: Journal of Systems and Control Engineering* 220 (2006), pp. 365–379. DOI: 10.1243/09596518JSCE183.

[10] I. S. Pearsall. "Acoustic detection of cavitation." In: *Proceedings of the Institution of Mechanical Engineers* 181 (1966), paper 14.

[11] P. J. McNulty and I. S. Pearsall. "Cavitation inception in pumps." In: *Journal of Fluids Engineering* 104.1 (1982), pp. 99–104.

[12] J. D. Smith. *Gear Noise and Vibration*. CRC Press, 1999, p. 181.

[13] C. Bonacini. "Sulle pompe a ingranaggi a dentatura elicoidale." In: *Tecnica Italiana* 3 (1965).

[14] I. E. Idel'chik. *Handbook of hydraulic resistance*. Ed. by Jaico Pub House. 3rd. 2001, p. 790.

[15] P. Casoli, A. Vacca, and G. Franzoni. "A numerical model for the simulation of external gear pumps." In: *6th JFPS International symposium on Fluid Power*. 2005, pp. 705–710.

[16] E. Mucchi, G. Dalpiaz, and A. Fernandez Del Rincon. "Elasto-dynamic analysis of a gear pump–Part IV: Improvement in the pressure distribution modelling." In: *Mechanical Systems and Signal Processing* (2014), pp. 1–21. DOI: 10.1016/j.ymssp.2014.05.049.

[17] E. Mucchi, G. Dalpiaz, and A. Fernandez Del Rincon. "Elastodynamic analysis of a gear pump. Part I: Pressure distribution and gear eccentricity." In: *Mechanical Systems and Signal Processing* 24.7 (2010), pp. 2160–2179. DOI: 10.1016/j.ymssp.2010.02.003.

[18] E. Mucchi, G. Dalpiaz, and A. Rivola. "Elastodynamic analysis of a gear pump. Part II: Meshing phenomena and simulation results." In: *Mechanical Systems and Signal Processing* 24.7 (2010), pp. 2180–2197. ISSN: 08883270. DOI: 10.1016/j.ymssp.2010.02.004.

[19] E. Mucchi and G. Dalpiaz. "Elasto-dynamic analysis of a gear pump–Part III: Experimental validation procedure and model extension to helical gears." In: *Mechanical Systems and Signal Processing* 50-51 (2015), pp. 174–192. DOI: 10.1016/j.ymssp.2014.05.048.

[20] E. Mucchi, G. Dalpiaz, and A. Rivola. "Dynamic behavior of gear pumps: Effect of variations in operational and design parameters." In: *Meccanica* 46.6 (2011), pp. 1191–1212. DOI: 10.1007/s11012-010-9376-y.

[21] G. Dalpiaz, A. Fernandez Del Rincon, E. Mucchi, and A. Rivola. "Model-Based Analysis of Dynamic Phenomena in Gear Pumps." In: *5th International Conference on Acoustical and Vibratory Surveillance Methods and Diagnostic Techniques*. Senlis, France, 2004. DOI: 10.1007/s13398-014-0173-7.2.

[22] E. Mucchi, A. Rivola, and G. Dalpiaz. "Modelling dynamic behaviour and noise generation in gear pumps: Procedure and validation." In: *Applied Acoustics* 77 (2014), pp. 99–111. DOI: 10.1016/j.apacoust.2013.10.007.

[23] R.J. Comparin and R. Singh. "Non-linear frequency response characteristics of an impact pair." In: *Journal of Sound and Vibration* 134.2 (1989), pp. 259–290. DOI: 10.1016/0022-460X(89)90652-4.

[24] A. Kahraman and R. Singh. "Non-linear dynamics of a spur gear pair." In: *Journal of Sound and Vibration* 142.1 (1990), pp. 49–75. DOI: 10.1016/0022-460X(90)90582-K.

[25] S. Theodossiades and S. Natsiavas. "Non-Linear dynamics of gear-pair systems with periodic stiffness and backlash." In: *Journal of Sound and Vibration* 229.2 (2000), pp. 287–310. DOI: 10.1006/jsvi.1999.2490.

[26] S. Theodossiades and S. Natsiavas. "On geared rotordynamic systems with oil journal bearings." In: *Journal of Sound and Vibration* 243.4 (2001), pp. 721–745. DOI: 10.1006/jsvi.2000.3430.

[27] A. Kahraman and R. Singh. "Error Associated with a Reduced Order Linear Model of a Spur Gear." In: *Journal of Sound and Vibration* 149 (1991), pp. 495–498.

[28] A. Kahraman and G. W. Blankenship. "Experiments on nonlinear dynamic behavior of an oscillator with clearance and periodically time-varying parameters." In: *Journal of Applied Mechanics* 64.1 (1997), pp. 217–226. ISSN: 0021-8936.

[29] M. R. Kang and A. Kahraman. "Measurement of vibratory motions of gears supported by compliant shafts." In: *Mechanical Systems and Signal Processing* 29 (2012), pp. 391–403. DOI: 10.1016/j.ymssp.2011.11.007.

[30] A. Kahraman and R. Singh. "Non-linear dynamic of a geared rotor-bearing system with multiple clearances." In: *Journal of Sound and Vibration* 144.3 (1991), pp. 469–506.

[31] A. Kahraman, H. Ozguven, and D.R. Houser. "Dynamic analysis of geared rotors by finite elements." In: *Journal of Mechanical Design* 114.September (1992), pp. 507–514. DOI: 10.1115/1.2926579.

[32] M. Kubur, A. Kahraman, D. M. Zini, and K. Kienzle. "Dynamic Analysis of a Multi-Shaft Helical Gear Transmission by Finite Elements: Model and Experiment." In: *Journal of Vibration and Acoustics* 126.3 (2004), p. 398. DOI: 10.1115/1.1760561.

[33] P. Velex and M. Maatar. "A mathematical model for analyzing the influence of shape deviations and mounting errors on gear dynamic behaviour." In: *Journal of Sound and Vibration* 191.5 (1996), pp. 629–660. DOI: 10.1006/jsvi.1996.0148.

[34] G. Sika and P. Velex. "Instability analysis in oscillators with velocity-modulated time-varying stiffness-Applications to gears submitted to engine speed fluctuations." In: *Journal of Sound and Vibration* 318.1-2 (2008), pp. 166–175. DOI: 10.1016/j.jsv.2008.04.008.

[35] A. Vacca and M. Guidetti. "Modelling and experimental validation of external spur gear machines for fluid power applications." In: *Simulation Modelling Practice and Theory* 19.9 (2011), pp. 2007–2031. DOI: 10.1016/j.simpat.2011.05.009.

[36] G. Miccoli and P. Vagnoni. "Determinazione per via sperimentale dei carichi sul corpo di una pompa ad ingranaggi esterni." In: *Oleodinamica Pneumatica* 11 (1988), pp. 145–155.

[37] D. McCandlish and R. E. Dorey. "The mathematical modelling of hydrostatic pumps and motors." In: *Proceedings of the Institution of Mechanical Engineers, Part B: Management and Engineering Manufacture* 198.3 (1984), pp. 165–174. DOI: 10.1243/PIME_PROC_1984_198_062_02.

[38] W.M.J. Schlosser. "Mathematical model for displacement pumps and motors." In: *Hydraulic Power Transmission* 7 (1961), pp. 252–257.

[39] D. Thiagarajan and A. Vacca. "Investigation of hydro-mechanical losses in external gear machines: simulation and experimental validation." In: *BATH/ASME 2016 Symposium on Fluid Power and Motion Control*. Bath, UK, 2016, pp. 1–10.

[40] R. Singh and H. Xie. "Analysis of Automotive Neutral Gear Rattle." In: *Journal of Sound and Vibration* 131.2 (1989), pp. 177–196.

[41] N. D. Manring and S. B. Kasaragadda. "The Theoretical Flow Ripple of an External Gear Pump." In: *Journal of Dynamic Systems, Measurement, and Control* 125.3 (2003), pp. 396–404. DOI: 10.1115/1.1592193.

[42] F. K. Orcutt and E. B. Arwas. "The Steady-State and Dynamic Characteristics of a Full Circular Bearing and a Partial Arc Bearing in the Laminar and Turbulent Flow Regimes." In: *Journal of Lubrication Technology* 89.2 (1967), p. 143. DOI: 10.1115/1.3616932.

[43] Tsuneo Someya. *Journal-Bearing Databook*. Ed. by Tsuneo Someya. 1989.

[44] K. Foster, R. Taylor, and M. Bidhendi. "Computer Prediction of Cyclic Excitation Sources for an External Gear Pump." In: *Proceedings of the Institution of Mechanical Engineers. Part B: Management and engineering manufacture* 199.3 (1985), pp. 175–180. DOI: 10.1017/CBO9781107415324.004.

[45] S. Mancò and N. Nervegna. "Simulation of an external gear pump and experimental verification." In: *JHPS. International symposium on fluid power*. Tokyo, 1989.

[46] C. Bonacini and M. Borghi. "Calcolo delle pressioni nei vani fra i denti di una macchina oleodinamica ad ingranaggi esterni." In: *Oleodinamica Pneumatica* 11 (1990), pp. 128–134.

[47] S. Falfari and P. Pelloni. "Setup of a 1D model for simulating dynamic behaviour of external gear pumps." In: *SAE International*. Rosemont, Illinois, 2007.

[48] M. Borghi, M. Milani, F. Paltrinieri, and B. Zardin. "The Influence of Cavitation and Aeration on Gear Pumps and Motors Meshing Volumes Pressures." In: *ASME IMECE 2006*. Chicago, 2006, pp. 1–10.

[49] J. Zhou, A. Vacca, and P. Casoli. "A novel approach for predicting the operation of external gear pumps under cavitating conditions." In: *Simulation Modelling Practice and Theory* 45 (2014), pp. 35–49. DOI: 10.1016/j.simpat.2014.03.009.

[50] R. H. Frith and W. Scott. "Comparison of an external gear pump wear model with test data." In: *Wear* 196 (1996), pp. 64–71.

[51] E. Koç, A. O. Kurban, and C. J. Hooke. "An analysis of the lubrication mechanisms of the bush-type bearings in high pressure pumps." In: *Tribology International* 30.8 (1997), pp. 553–560.

[52] E. Koç. "Bearing misalignment effects on the hydrostatic and hydrodynamic behaviour of gears in fixed clearance end plates." In: *Wear* 73.1/2 (1994), pp. 199–206.

[53] E. Koç and C. J. Hooke. "An experimental investigation into the design and performance of hydrostatically loaded floating wear plates in gear pumps." In: *Wear* 209 (1997), pp. 184–192.

[54] F. Paltrinieri, M. Milani, and M. Borghi. "Modelling and simulating hydraulically balanced external gear pumps." In: *2nd International FPNI Ph.D. Symposium on Fluid Power*. 2002.

[55] M. Borghi, M. Milani, F. Paltrinieri, and B. Zardin. "Studying the axial balance of external gear pumps." In: *SAE International* (2005). DOI: 10.4271/2005-01-3634.

[56] S. Dhar and A. Vacca. "A novel CFD – Axial motion coupled model for the axial balance of lateral bushings in external gear machines." In: *Simulation Modelling Practice and Theory* 26 (2012), pp. 60–76. ISSN: 1569190X. DOI: 10.1016/j.simpat.2012.03.008.

[57] R. Castilla, P. J. Gamez-Montero, N. Ertrk, A. Vernet, M. Coussirat, and E. Codina. "Numerical simulation of turbulent flow in the suction chamber of a gearpump using deforming mesh and mesh replacement." In: *International Journal of Mechanical Sciences* 52.10 (2010), pp. 1334–1342. DOI: 10.1016/j.ijmecsci.2010.06.009.

[58] D. del Campo, R. Castilla, G. A. Raush, P. J. Gamez-Montero, and E. Codina. "Numerical Analysis of External Gear Pumps Including Cavitation." In: *Journal of Fluids Engineering* 134.8 (2012), p. 081105. DOI: 10.1115/1.4007106.

[59] R. Castilla, P. J. Gamez-Montero, D. del Campo, G. Raush, M. Garcia-Vilchez, and E. Codina. "Three-Dimensional Numerical Simulation of an External Gear Pump With Decompression Slot and Meshing Contact Point." In: *Journal of Fluids Engineering* 137 (2015), p. 041105. DOI: 10.1115/1.4029223.

[60] Y. Yoon, B. H. Park, J. Shim, Y. O. Han, and S. H. Yun. "Numerical simulation of three-dimensional external gear pump using immersed solid method." In: *Applied Thermal Engineering* (2017).

[61] M. Rundo. "Models for Flow Rate Simulation in Gear Pumps: A Review." In: *Energies* 10.9 (2017), p. 1261. DOI: 10.3390/en10091261.

[62] T. Ichikawa and K. Yamaguchi. "On pulsation of delivery pressure of gear pump." In: *Bulletin of the Japan Society of Mechanical Engineers* 14 (1971), pp. 1304–1312.

[63] K. J. Huang and W. C. Lian. "Kinematic flowrate characteristics of external spur gear pumps using an exact closed solution." In: *Mechanism and Machine Theory* 44.6 (2009), pp. 1121–1131. DOI: 10.1016/j.mechmachtheory.2008.10.002.

[64] R. S. Devendran and A. Vacca. "Design potentials of external gear machines with asymmetric tooth profile." In: *Proceedings of the ASME/BATH 2013 Symposium on Fluid Power & Motion Control*. 2013, pp. 1–12.

[65] R. S. Devendran and A. Vacca. "Theoretical analysis for variable delivery flow external gear machines based on asymmetric gears." In: *Mechanism and Machine Theory* 108 (2017), pp. 123–141. DOI: 10.1016/j.mechmachtheory.2016.10.001.

[66] A. Meldahl. *Théorie des pompes a engrenages*. Ed. by Revue Brown Boveri. 1939.

[67] Y. Takahashi. "On the trapping of fluid between the teeth of the involute gear pump." In: *Transaction of the Japan Society of Mechanical Engineers* 3.6 (1940), pp. 6–10.

[68] B. Zardin, F. Paltrinieri, M. Borghi, and M. Milani. "About the prediction of pressure variation in the inter-teeth volumes of external gear pumps." In: *Proceedings of the 3rd FPNI - PhD Symposium on Fluid Power*. Terrassa, Spain, 2004.

[69] X. Song, H. G. Wood, S. W. Day, and D. B. Olsen. "Studies of Turbulence Models in a Computational Fluid Dynamics Model of a Blood Pump." In: *Artificial Organs* 27.10 (2003), pp. 935–937. DOI: 10.1046/j.1525-1594.2003.00025.x.

[70] C. Buratto, M. Pinelli, P. R. Spina, A. Vaccari, and C. Verga. "Cfd Study on Special Duty Centrifugal Pumps Operating With Viscous and Non-Newtonian Fluids." In: *European Turbomachinery Conference* 1 (2015), pp. 1–13.

[71] J. C. Chang, C. W. Chang, T. C. Hung, J. R. Lin, and K. C. Huang. "Experimental study and CFD approach for scroll type expander used in low-temperature organic Rankine cycle." In: *Applied Thermal Engineering* 73.2 (2014), pp. 1444–1452. DOI: 10.1016/j.applthermaleng.2014.08.050.

[72] Y. Bastani and M. de Queiroz. "A new analytic approximation for the hydrodynamic forces in finite-length journal bearings." In: *Journal of Tribology* 132.1 (2009), 014502 [1]–014502 [9].

[73] B. J. Hamrock. *Fundamentals of Fluid Film Lubrication*. New York, NY: McGraw-Hill, 1994.

[74] A. Harnoy. *Bearing Design in Machinery: Engineering Tribology and Lubrication*. Ed. by Marcel Dekker. New York, NY, 2003.

[75] G. B. DuBois and F. W. Ocvirk. *Analytical Derivation and Experimental Evaluation of short-Bearing Approximation for Full Journal Bearings*. Tech. rep. 1953, pp. 1199–1206.

[76] D. Childs, H. Moes, and H. van Leeuwen. "Journal bearing impedance descriptions for rotordynamic applications." In: *Journal of Lubrication Technology* (1977), pp. 198–214.

[77] D. Talbot, A. Kahraman, and S. Seetharaman. "A helical gear pair pocketing power loss model." In: *Journal of Tribology* 136 (2014).

[78] N. D. Manring. "Measuring Pump Efficiency: Uncertainty Considerations." In: *Journal of Energy Resources Technology* 127.4 (2005), p. 280. DOI: 10.1115/1.1926311.

[79] G. L. Zarotti and N. Nervegna. "Pump efficiencies approximation and modelling." In: *6th International Fluid Power Symposium*. Hannover, 1981, pp. 145–164.

[80] Jaroslav Ivantysyn and Monika Ivantysynova. *Hydrostatic pumps and motors: principles, design, performance, modelling, analysis, control and testing*. First Engl. New Delhi, India: Tech Books International, 2003, p. 512.

[81] R. Castilla, P. J. Gamez-Montero, G. Raush, and E. Codina. "Method for Fluid Flow Simulation of a Gerotor Pump Using OpenFOAM." In: *Journal of Fluids Engineering* 139.November (2017), p. 111101. DOI: 10.1115/1.4037060.

[82] E. Frosina, A. Senatore, and M. Rigosi. "Study of a High-Pressure External Gear Pump with a Computational Fluid Dynamic Modeling Approach." In: *Energies* 10.8 (2017), p. 1113. DOI: 10.3390/en10081113.

[83] S. Mancò and N. Nervegna. "Pressure transients in an external gear hydraulic pump." In: *Fluid Power* (1993).

[84] E. Mucchi, G. Cremonini, S. Delvecchio, and G. Dalpiaz. "On the pressure ripple measurement in variable displacement vane pumps." In: *Journal of Fluids Engineering* 135 (2013), p. 091103.

[85] P. A. Abbot. "Cavitation detection measurements on Francis and Kaplan hydro turbines." In: *Proceedings of the Third International Symposium on Cavitation, Noise and Erosion in Fluid Systems*. Ed. by R. E. A. Arndt, M. L. Billet, and W. K. Blake. San Francisco, CA, 1989, pp. 55–61.

[86] P. A. Abbot, C. J. Gedney, and D. L. Greeley. "Cavitation monitoring of two axial-flow hydroturbines using novel acoustic and vibration methods." In: *Proceedings of the 13th IAHR Symposium*. Vol. 1. Montreal, Canada, 1986, paper 23.

[87] X. Escaler, E. Egusquiza, M. Farhat, F. Avellan, and M. Coussirat. "Detection of cavitation in hydraulic turbines." In: *Mechanical Systems and Signal Processing* 20.4 (2006), pp. 983–1007. DOI: 10.1016/j.ymssp.2004.08.006.

[88] T. Rus, M. Dular, B. Sirok, M. Hocevar, and I. Kern. "An Investigation of the Relationship Between Acoustic Emission, Vibration, Noise, and Cavitation Structures on a Kaplan Turbine." In: *Journal of Fluids Engineering* 129.September (2007), p. 1112. DOI: 10.1115/1.2754313.

[89] M. Čudina. "Detection of Cavitation Phenomenon in a Centrifugal Pump Using Audible Sound." In: *Mechanical Systems and Signal Processing* 17.6 (2003), pp. 1335–1347. DOI: 10.1006/mssp.2002.1514.

[90] M. Čudina and J. Prezelj. "Detection of cavitation in operation of kinetic pumps. Use of discrete frequency tone in audible spectra." In: *Applied Acoustics* 70.4 (2009), pp. 540–546. DOI: 10.1016/j.apacoust.2008.07.005.

[91] A. Adamkowski, A. Henke, and M. Lewandowski. "Resonance of torsional vibrations of centrifugal pump shafts due to cavitation erosion of pump impellers." In: *EFA* 70 (2016), pp. 56–72. DOI: 10.1016/j.engfailanal.2016.07.011.

[92] Zhaoli Yan, Jin Liu, Bin Chen, Xiaobin Cheng, and Jun Yang. "Fluid cavitation detection method with phase demodulation of ultrasonic signal." In: *Applied Acoustics* 87 (2015), pp. 198–204. DOI: 10.1016/j.apacoust.2014.07.007.

[93] Pankaj P. Gohil and R. P. Saini. "Effect of temperature, suction head and flow velocity on cavitation in a Francis turbine of small hydro power plant." In: *Energy* 93 (2015), pp. 613–624. DOI: 10.1016/j.energy.2015.09.042.

[94] M. M. Stopa, B. J. Cardoso Filho, and C. B. Martinez. "Incipient detection of cavitation phenomenon in centrifugal pumps." In: *IEEE Transactions on Industry Applications* 50.1 (2014), pp. 120–126. DOI: 10.1109/TIA.2013.2267709.

[95] J. Zhou, A. Vacca, and B. Manhartsgruber. "A Novel Approach for the Prediction of Dynamic Features of Air Release and Absorption in Hydraulic Oils." In: *Journal of Fluids Engineering* 135.9 (2013), p. 091305. DOI: 10.1115/1.4024864.

[96] A. K. Singhal, M. M. Athavale, H. Li, and Y. Jiang. "Mathematical Basis and Validation of the Full Cavitation Model." In: *Journal of Fluids Engineering* 124.3 (2002), p. 617. DOI: 10.1115/1.1486223.

[97] D. del Campo, R. Castilla, G. A. Raush, P. J. Gamez-Montero, and E. Codina. "Pressure effects on the performance of external gear pumps under cavitation." In: *Proceedings of the Institution of Mechanical Engineers, Part C: Journal of mechanical engineering science* 228.16 (2014), pp. 2925–2937.

[98] Y. Liu, L. Wang, and Z. Zhu. "Experimental and numerical studies on the effect of inlet pressure on cavitating flows in rotor pumps." In: *Journal of Engineering Research* 4.2 (2016), pp. 151–171. DOI: 10.7603/s40.

[99] Dario Buono, Daniela Siano, Emma Frosina, and Adolfo Senatore. "Gerotor pump cavitation monitoring and fault diagnosis using vibration analysis through the employment of auto-regressive-moving-average technique." In: *Simulation Modelling Practice and Theory* 71 (2016), pp. 61–82. DOI: 10.1016/j.simpat.2016.11.005.

[100] J. B. Hunt, A. J. Ryde-Weller, and F. A. H. Ashmead. "Cavitation between meshing gear teeth." In: *Wear* 71.1 (1981), pp. 65–78.

[101] J Paul Tullis. *Hydraulics of Pipelines - Pumps, Valves, Cavitation, Transients*. John Wiley & Sons, Inc., 1989, p. 266.

[102] Xian Wu Luo, Bin Ji, and Yoshinobu Tsujimoto. "A review of cavitation in hydraulic machinery." In: *Journal of Hydrodynamics* 28.3 (2016), pp. 335–358. DOI: 10.1016/S1001-6058(16)60638-8.

[103] S C Li. *Cavitation in hydraulic machinery*. London: Imperial College Press, 2000.